Your reference: wes-2025-233
Date: January 22, 2026

DTU Wind and Energy Systems
DTU Risø Campus
Frederiksborgvej 399
4000, Roskilde
Denmark

Subject: Author's Response
Wind Energy Science Journal
Reviewers

Dear Reviewers,

Thank you for your constructive comments on our paper. Your feedback helped us significantly improve our manuscript. This document presents our reply to the comments raised and provides an overview of the changes we made. The responses are shown in blue, and the related changes in the preprint are shown in red (the line numbering in "See lines" refers to the comparison document attached in the bottom of this document). The comparison manuscript is attached after the response to the reviewers, with the removed portions in red strikethrough and the added text in blue underlined text.

In summary, we have made an effort to reduce the length of the paper without missing important explanations and takeaways. The paper has been reduced from 28 pages to 26 pages, without increasing the Appendices. Considering further figure reductions due to two column format of WES, we expect the final publication could be shortened to around 24-25 pages. The preprint also has benefited from further grammatical corrections along the main text.

We agreed that key figures had to be increased and that inconsistencies were present in the original paper. We appreciate your criticism towards these and we have adjusted the paper accordingly. Additional redundancies found by the authors have also been removed. For example, Figures 3 and 5 (preprint) have been combined, presenting the drivetrain loads and its thermal model together. Similarly, Figure 8 (preprint) has been removed and the methodological steps for the simple uncertainty propagation exercise (Section 5.5.2) are explained in the text. The Discussion (Section 6) has been incorporated into the Results and Conclusion (Sections 5 and 7, respectively) as suggested by the Reviewer 1. Finally, Figure 15 and Equation 20 (both in the comparison and revised manuscript) have been added to support the claim made by the authors in the paper that low turbulence could increase the fatigue loads of a locating main bearing at rated wind speed, a phenomenon introduced as turbulence averaging and explained in Section 5.5.2.

Sincerely,
Bruno Rodrigues Faria
Nikolay Dimitrov
Nikhil Sudhakaran
Matthias Stammler
Athanasios Kolios
W.Dheelibun Remigius
Xiaodong Zhang
Asger Bech Abrahamsen

Enclosure(s):
- General remarks
- Response to Reviewer 1
- Response to Reviewer 2
- Marked-up version of the comparison manuscript

1 Response to Reviewer 1

In this paper, the authors describe a methodology to calculate the consumed fatigue life for a wind turbine main bearing and tower based on a combination of SCADA measurements, accelerometers, and dedicated strain gauge bridges and models. In general it is interesting, but the article could benefit a bit by further grammatical editing and trimming in length as it's quite long. The most interesting Figures 14-18 of results should be increased in size, as they are quite small even when zooming in electronically. I did not have the time or expertise to review the majority of the material on tower fatigue, including the entirety of sections 5.3 and 5.4. I offer the following comments for consideration to improve the article.

Response: The authors greatly appreciate the detailed and reasonable feedback. It has been fundamental to make the results related to the strain gauge calibration and main bearings analysis, and their respective takeaways, more consistent. The reference to Figure numbers refer to the comparison document attached in the bottom, which should match the updated draft numbering.

Revised Section: Figures 14-18 (Figures 12-16 in the reviewed paper) have been increased, with a smallest increment on Figure 18 (Figure 16 in the reviewed paper), since it was considered the least critical. The manuscript has been shortened by two pages while preserving all relevant findings. A breakdown of the modifications according to each feedback is presented in the following.

2 Comments and suggestions:

Abstract

- Line 19: I still have my doubts about the importance of "... low turbulence intensity..." mentioned here. See later comments on Section 5.5.2.

  Response: The authors agreed that this sentence was misleading the reader. In fact, the thrust curve is claimed to be the main driver of the fatigue loads in the locating main bearings. Whereas, for a critical operation condition, at rated wind speed (peak of the thrust curve), higher fatigue loads were mapped for low turbulence and low shear from 2016 to 2024 (inclusive). The authors claim that such effect is explained by a turbulence averaging of the turbine thrust curve and subsequent bearing dynamic load curve as function of the wind speed

  Revised Section: The final lines in the abstract have been modified to "Fatigue loads in the locating main bearing are driven by the peak of the turbine thrust curve but higher loads are observed on the main bearings at rated wind speed, most critical operation, with low turbulence intensity and low shear." More comments are adjusted in Section 5.5.2. The authors have also added one possible explanation to this observation, through the new Figure 15 and Equation 20. The effect is explained by the fact that that higher turbulence at rated wind speed, should flatten the peak of the thrust curve, and by so, decrease the fatigue loads of the locating main bearing.

  See lines: 20-25 and Figure 15

- Lines 21–22: Related to comments on Section 5.5.1, on the surface, I don't disagree with the statement "It was also found that the specification of the gearbox mounting stiffness can lead to a 60% overprediction of the main bearing loads" but it is misleading because it depends on one's view of the meaning of "specification" of the stiffness. In this case, the 60% overprediction is a result of comparing a realistic stiffness to a rigid gearbox mount, which is not a typical assumption as the elastomeric mounts are intentionally relatively soft. When the realistic stiffness is compared to no (or very low) mounting stiffness, there is very little difference in the main bearing loads. Although it's still worthy to describe in the body of the paper, from this perspective there is little interesting to note in the Abstract itself, so I recommend this sentence just be deleted.

  Response: The authors agreed that the mentioned sentences is not relevant enough to be included in the abstract. In addition, the main text has been reformulated so that the reader understands that only by applying a non realistic clamped gearbox mounting, the fatigue loads of the main bearings would be significantly affect. While, if the gearbox mounting is neglected in the drivetrain load model or considered flexible, within reasonable values found in literature, small impact should be observed on the main bearing loads.

Revised Section: The sentence in lines 23-24 has been removed and a better explanation in included in Section 5.5.1 "Figure 13 shows the effect of the stiffness used to model the gearbox mounting fixation points on the P_{eq} of the front and rear main bearing. Small variation is observed if the stiffness is neglected or used as in the literature. However, as shown in Figure 13, an overprediction of 10% and 60% of the front and rear dynamic equivalent loads P_{eq} could be reached if a gearbox is rigidly fixed in a 4-point drivetrain, which is not a realistic assumption."

See lines: 563-568

1 Introduction

- Line 35: Do the authors intend the phrase "As a failure in the main bearing means a failure in turbine operation" to mean that the turbine itself may fail catastrophically, or just lead to downtime and replacement? From the next sentences, it seems the latter. If so, I recommend "As a main bearing replacement incurs significant costs and turbine downtime, . . . "

  Response: Agreed.

  Revised Section: The sentence has been updated as suggested.

  See line: 38

- Line 54: I am not sure of the meaning of "aims to maximize coverage using". I think simply "aims to use" is clearer.

  Response: Agreed.

  Revised Section: The sentence has been updates as suggested.

  See line: 59

2.2 Main bearing fatigue lifetime

- Lines 130–134: In addition to the text here regarding a_ISO, I believe adding a pointer statement that a drivetrain thermal model will be discussed in Section 4.4 would be helpful. Without any such statement, the reader is left wondering how a_ISO will be determined (I did). Such a statement is also made in Section 4.0, but it would have been helpful earlier.

  Response: Agreed.

  Revised Section: A reference to the main bearing thermal model is also made in Section 2.2 in " In this work, a drivetrain thermal model is used to allow the estimation of $a_{\mathrm{ISO},j}$, as shown in Section 4.2.

  See lines: 151-152

2.3 Virtual load sensors

- Line 137: In general, the article seems to place emphasis on the benefit of "keeping the necessary measuring [instrumentation] in the nacelle." In this case, strain gauges in the nacelle rather than at the bottom of the tower. Is there really much benefit to this in practice though? Obviously, strain gauges at the tower bottom are very easily accessible. Can the authors comment?

  Response: The authors have decided to remove such emphasis from this paper. The discussion is interesting as it can be approached from a Original Equipment Manufacturer (OEM), an operator or a Retrofit partner point of view. However, it was decided to leave such subject for a next publication to come. The importance of the virtual load sensors is focused in terms of replacing physical sensor when they fail.

  Revised Section: The mentioned sentenced has been adjusted to remove the discussion on "keeping the necessary measuring instrumentation in the nacelle".

  See lines: 80-81

3 Measurements

- Line 166: There is no "...graph on the left...". The discussion here does have some importance, as in the Abstract the very high fatigue lives are attributed to "the low average wind speed of the turbine site compared to the wind turbine design wind class IA."

  Response: Thank you for the careful reading and feedback. The first sentence should have been removed during the updating of drafts.

  Revised Section: The first sentence has been removed, whereas the following discussion is still valid: "the Risø site has fairly low wind resources (...)".

  See lines: 185

- Lines 173 and 176: Maybe I am mistaken, but gamma is described as the yaw angle in line 170 but the azimuth angle in line 176.

  Response: Agreed.

  Revised Section: The gamma γ has been corrected to the phi φ to represent the azimuth angle.

  See line: 196

4.1 Strain gauge zero-drift automatic calibration

- Lines 208–209: I don't understand the meaning of "No external dynamic load should cause zero strain." I don't necessarily disagree with it, but it seems to be a restatement of the fact that the external loads are assumed to be zero in idling and parked conditions. Also, I recommend "bending moment" be changed to "bending moments" here, or even "blade root and tower bottom bending moments" for greater clarity.

  Response: The first mentioned sentence was misleading the reader. It was supposed to introduced the concept behind the calibration methods. However, it was decided to remove this sentence and leave the explanation of the calibration methods to be done in Section 4.1.1. The calibration is not directly connected to the presence or absence of external loads, but by the consistent variations of defined gravitational loads. As for the second mentioned sentence, the authors agreed.

  Revised Section: The first mentioned sentence has been removed. And the reader could refer to Section 4.1.1 to have a better understanding of the calibration methods. The second mentioned sentence has been updated as suggested.

  See lines: 228

4.2 From blade and tower to main bearing loads

- Line 233: I believe adding a pointer "A sensitivity analysis is performed in Section 5.5.1 to evaluate the importance of this assumption" would be helpful.

  Response: Agreed.

  Revised Section: The suggested sentence has been added in Section 4.2.

  See lines: 254-255

- Lines 246–251: Here the drivetrain model is discussed, which assumes that the gearbox carries some load because of the main shaft bending flexibility. This may very well be fine, but I'll admit I don't know off the top of my head how good of an assumption this is compared to deflections resulting from main bearing internal radial clearance.

  Response: The authors appreciate the raised discussion. Indeed radial clearance was not mentioned initially. The validation of such assumption would not be feasible in the scope of this paper. However, the authors reason that, considering the flexible gearbox mounting usually seen in operation, neglecting the radial clearance is in the more conservative side of this analysis.

Revised Section: The authors have added in Section 4.2. " The radial clearance from the bearings is not explicitly considered." for the sake of completeness. However, no further validations were pursued.

See line: 268-269

- Line 257: Here, thrust load-sharing between the two main bearing is discussed, but in the end I believe the rear bearing is simply assumed to act as the locating bearing and carry all the thrust. This would be a common design objective achieved by greater axial internal clearance in the front than the rear bearing. Is that a correct understanding of what the authors have implemented?

  Response: Exactly. The authors appreciated this comments as it makes it more clear to the reader the decision that the rear main bearing is the locating bearing.

  Revised Section: The following sentence has been added in Section 4.2 "Since both bearings can carry axial loads, the system may become over-constrained, causing additional axial stress during thermal expansion. For these reasons, the rear bearing is considered the locating bearing, being the larger bearing and with greater axial internal clearance."

  See lines: 279-282

4.3 Tower bottom virtual load sensor: thrust and fatigue loads

- Figure 4: Is quite small. I recommend each one be enlarged. Additionally, I'm not sure I understand the value of examining the PSD of the azimuth. I assume this signal looks similar to a triangular wave (i.e. roughly linear from 0 to 360 degrees repeating for each complete rotor revolution), so it has spectral content at each rotor frequency, not just 1, 3, and 6P as described in line 279.

  Response: Agreed. The authors have initially added the azimuth angle φ as the measured azimuth angle less the integral of rotor speed ω in time. However, it was decided that this exercise did not add relevant discussion in the main text, in comparison to the remaining input signals (SCADA, nacelle accelerometer, blade root strain gauges).

  Revised Section: Figure 4 has been increased and the azimuth angle φ has been removed from Figure 4(left). And lines 325-327 has been removed as it was an erroneous explanation of the frequency components in the azimuth angle φ.

  See lines: 325-327 and Figure 4

- Line 280: I don't understand the sentence "... only the accelerometer signal can well capture the first fore-aft turbine frequency (around 0.62 Hz Rinker et al. (2018)), while its amplification of higher frequency components compared to $M_{fore-aft}$ cannot be considered pure electrical noise." To me, it appears that there is nearly as strong content of this frequency in $M_{fore-aft}$ as the accelerometer as shown in the middle figure.

  Response: The authors have not properly explained the scope of Figure 4: present the input signal Power Spectrum Density (PSD) of the virtual load sensors compared to the target variable PSD $M_{fore-aft}$ (tower bottom bending moment in the fore-aft direction). As the latter would not be available in the deployment of the virtual load sensors.

  Revised Section: The authors have added explicitly that the $M_{fore-aft}$ refers to the target variable in the training of the virtual load sensor, in then it would be interesting to compare its PSD with all different input sources (SCADA, nacelle accelerometer and blade root strain gauges). Added as "The black line is added in all charts as is the target variable $M_{fore-aft}$ of the virtual load sensors."

  See lines: caption of Figure 4

- Line 284: Gearbox vibrations are described relative to the accelerometer measurement; however, I don't believe it's described or shown in the paper where exactly this accelerometer is located. Is it attached to the bedplate, for instance? I don't necessarily disagree with the statement here; however, the vibration frequencies in these plots are from 0 to 5 Hz or so, which is quite low for a "gearbox vibration" in general, for instance, as a result of tooth meshing. More importantly though, what is the significance of the extent of attenuation (or not) of the accelerometer compared

to Mfore-aft? If there isn't any significance, then why is this discussed? If there is significance, what is it?

Response: The authors agree that the location of the nacelle accelerometer was not previously stated. Secondly, the extent of the attenuation of the accelerometer compared to the $M_{fore-aft}$ could add undesired oscillation into the virtual load sensor estimate of the $M_{fore-aft}$ when trying to the minimize the training error with non related oscillations.

Revised Section: The authors have defined the position of the nacelle acceleration and explicitly stated a possible impact of it in the virtual load sensor performance as in "The most consistent explanation is that the gearbox operation feeds high-frequency broadband vibrations to the nacelle accelerometer mounted below the bedplate near the gearbox. Virtual load sensors trained on the nacelle accelerometer might add higher frequency oscillations to the $M_{fore-aft}$ estimate, as shown in Figure (...)."

See lines: 331-335

4.4 Drivetrain thermal model

- In general, the thermal model described here is interesting. Aside from the statement "... it yielded 3 C MAE" for the gearbox temperature, I don't have a good sense of the actual temperature results. I see this is later included in Section 5.5.4, so I am wondering why this mention of 3 C MAE is included in the Methodology section rather than the Results section. Having said that, I think practically speaking such a thermal model might not be needed as many or most turbines have an existing main bearing temperature measurement.

  Response: Indeed, the mentioning on the MAE is misplaced and have been moved to the Results. And the authors agreed that main bearing temperature are often available and have added a note on that.

  Revised Section: The error in the gearbox temperature MAE has been moved to Section 5.5.3. And the authors have added in the beginning of the "Drivetrain thermal model" subsection "In case the temperature measurements of the main bearings are not available, estimates of the temperature of the main bearings are necessary to incorporate the life modification factor a_{ISO}." to make it clear that the drivetrain thermal model is implemented since main bearing temperatures were not available in the DTU research V52 turbine.

  See lines: 284-285 and 615

- Line 312: Here, the grease cleanliness level is mentioned, but what assumption was made about it? Typical contamination maybe?

  Response: The authors agree that assumptions taken on the grease cleanliness should be stated. But since this study has used different assumptions in Figures 15 and 16, it was decided to mentioned the section in which this assumption is made.

  Revised Section: A referral to Section 5.5.3 has been added.

  See lines: 304

5.1 Continual calibration routines

- Line 322: Here it is stated "From the left charts, it is possible to observe larger zero drifts for the blade root compared to the tower bottom strain gauges." This may be true, but it is quite difficult to tell as the channels have offsets that overshadow any change in them over time. A better way to show the drift would be to normalize each one by their initial value and plot the change over time.

  Response: Agreed.

  Revised Section: The mean value of the offset from the left chart in Figure 5a has been subtracted to facilitate the visualization. Whereas the offsets in Figure 5b have been maintained as it was already possible to visualize drift and at a similar bending moment range as of Figure 5a (around 500 kNm).

  See lines: Figure 5a(left) and caption.

5.2.1 Fatigue damage accumulation

- I thought I understood how the lifetimes of the tower (1770 years) and front (166 years) and rear (333 years) were determined, but apparently not. For example, I had assumed if 0.003 D is accumulated in the tower in 9 years, then it would take 3,000 years (= 9/0.003) for D to reach a value of 1. Similarly for the main bearings (9/0.03 = 300 years for the front bearing). It's not clear to me that Equations 2 and 7 explain this difference. If the authors could address how the stated lifetimes are calculated, I believe it would be beneficial.

  Response: Agreed. Once again, the authors appreciated the careful reading. This has been a mistake in the documentation of the calculated values.

  Revised Section: The reviewers have estimated the corrected values. The tower lifetime is calculated as 2952 years, and the front and rear main bearings lifetime is calculated as 282 and 566 years, respectively. This has been updated both in the abstract and main text.

  See lines: 10 and 410-411

5.2.3 Effect of periodic calibration on the main bearings L10

- Line 361: I recommend adding "... can influence the lifetime estimation of main bearings for this methodology."

  Response: Agreed. This should emphasize that the absolute errors in the L_{10} due to periodic calibration are valid for the proposed methodology.

  Revised Section: The sentence has been updated as suggested.

  See lines: 437

5.5 Main bearings loads and fatigue lifetime analysis

- Figure 14 especially would benefit from increasing in size.

  Response: Agreed. Figure 12 (previous Figure 14) has been increased to facilitate visualization. However due to the final size of the document, further increasing was not possible.

  Revised Section: Figure 12 (previous Figure 14) has been increased while keeping it in a two-column fitting.

  See lines: refer to Figure 12.

5.5.1 Sampling frequency and gearbox mounting stiffness assumptions

- Although on the surface I don't disagree with Figure 15b or the statement that "overprediction of the front and rear dynamic equivalent loads could be reached, if a gearbox is assumed to be rigidly fixed in a 4-point drivetrain" in line 451, the "baseline" that is being compared to for this paper is a baseline of rigid stiffness of the gearbox mounts, which I don't know is a very common assumption. This results in (large sounding) overpredictions of up to 60%. I think it's much more common to do the opposite: that is, neglect the stiffness of these mounts as a "baseline" for a simple model (which is the description used in the Conclusions), which when comparing the estimated stiffness to would result in a very similar prediction. The conclusion one would derive then sounds quite a bit different. It would be that the dynamic equivalent loads are not affected (or only affected by a very small amount, it depends on the actual numbers in Figure 15b) by the estimated gearbox mounting stiffness compared to an assumption of no stiffness. This then makes the statement in Line 449–450 "... the assumption on which stiffness should be used to model the gearbox mounting fixation points into the bedplate has been shown to be one order of magnitude more relevant" to ring hollow. See related comments to Abstract and Conclusions.

  Response: The authors agreed that the text was misleading the reader into considering the baseline as the rigidly fixed. The previous mentioning to the gearbox mounting stiffness has been removed from the abstract and conclusion, as this exercise should be seen as a minor sensitivity analysis rather than a main outcome. In addition, in the sensitivity analysis section, the text has been adjusted as suggested by the reviewer.

Revised Section: The description of the sensitivity analysis has been adjusted to: "Figure 13 shows the effect of the stiffness used to model the gearbox mounting fixation points on the P_{eq} of the front and rear main bearing. Small variation is observed if the stiffness is neglected or used as in the literature (Haastrup et al., 2011; Keller et al., 2016). However, as shown in Figure 13, an overprediction of 10% and 60% of the front and rear dynamic equivalent loads P_{eq} could be reached if a gearbox is rigidly fixed in a 4-point drivetrain, which is not a realistic assumption."

See lines: 563-568

5.5.2 Environmental and operational conditions (EOCs) mapping of the main bearings dynamic equivalent loads

- To be honest, I had quite a difficult time discerning what the take-aways are from Figure 16 compared to Figure 14 discussed in all of Section 5.5.2. Are there any? In reading the text, I found myself more easily referring to Figure 14 for interpretation. Figure 14 tells me that Peq for both bearings is relatively well tightly grouped between the 10th and 90th percentiles, regardless of the shear or TI. Section 5.5.2 seems to try to convince me of the opposite. As an example for the rear bearing, let's take the sentence "Approximately 10% increase in load driven by a change in turbulence from 15% to 8%." Although this may be true, what is the significance? From what I can tell from Figure 16, what is described here is the small change from yellow to yellow-ish green. Is that correct? Another reason I bring this up is that the manuscript is already quite long, and I do not see anything new in Section 5.5.2. As far as I can tell, it could be deleted and any additional explanation included in the discussion of Figure 14. All Figure 16 seems to tell me that is new is that the TI is up to 30% and the shear coefficient up to 0.4, and that the highest values of Peq for the front bearing are at low shear (this latter fact has already been described elsewhere). It is only modestly interesting that the Peq for the front bearing tends to be largest around 10% TI, but then again it's a relatively small increase (maybe 20 kN out of over 200, or less than 10%) and it may be an artifact of averaging over 10 minutes. If this section and Figure 16 remains, Figure 16 especially would benefit from increasing in size.

  Response: Figure 14 (previous Figure 16) has been increased to facilitate visualization. The authors agreed that the draft discussion of the results in Figure 14 were misleading by not first introducing the impact of the thrust curve in the fatigue load P_{eq} of the locating main bearing. And then, discussing the impact of the turbulence intensity and shear. The authors have reformulated the description of Figure 14 to incorporate the feedback from the reviewer while allowing further discussion of the effect of the low turbulence. Similarly, the takeaways have been adjusted in the Abstract and Conclusion. The authors argue that the mapping of the fatigue loads measurements from 2016 to 2024 (inclusive) have presented a similar effect of the turbulence and shear in the fatigue loads of the locating main bearing at the rated wind speed.

  Revised Section: Figure 14 (previous Figure 16) has been increased while keeping it in a two-column fitting. And the last paragraph from Section 5.5.2 has been reformulated to "Note that the peak of the thrust curve is claimed to be the main driver of the fatigue load in the locating bearing $P_{eq,r}$ (Kenworthy et al., 2024; Quick et al., 2025). Figure 15 highlights the effect of the low turbulence intensity and shear at the rated wind speed, as they refer to the most damaging operating conditions and should affect the main bearing lifetime more severely depending on the probability of occurrence, as described in Equation 6".

  See lines: Figures 14 and 15

5.5.3 Main bearing lifetime using thrust estimate from virtual load sensors

- Line 474–475: I think this sentence would benefit from rewording to something like "This might come from the fact that the bearing fatigue is dominated by the mean value of Peq rather than fluctuations in the radial and/or axial loads."

  Response: Agreed. However the authors have decided to remove Section 5.5.3, as it was not a main learning from the paper and it could shorten the overall size of the publication.

  Revised Section: The suggested sentence has been included in Section 5.5.

  See lines: 549-552

5.5.4 Main bearings modified rating life: L10m and a_ISO

- Line 479: Here max main bearing temps of 55 and 61 C are mentioned, but what is shown in Figure 17 is ambient temps? Is there a reason for this? Why bother to calculate the main bearing temps if they are not to be shown in Figure 17, only discussed in general? It's the bearing temperature that really matters.

  Response: The authors agreed that the main bearing temperature have not been further mentioned. The authors have included the bearing temperature of the main bearing in pointers in Figure 15 (previous Figure 17). In addition, the minimum, average and maximum temperatures of the main bearings have been included in the main text. However, the authors argue that it might be more valuable to the current analysis to map the bearing lifetime as function of external environmental conditions rather than subsequent physical quantities that are analytically linked to the main bearing lifetime such as P_{eq}, viscosity ratio κ or bearing temperature T_f and T_r. A figure mapping the L_{10m} as function of the main bearing temperature could also lead to good discussion but has been avoided to shorten the length of the paper.

  Revised Section: The minimum, average and maximum temperatures of the main bearings have been included in the main text. And the temperature of the main bearings have been added in Figure 16.

  See lines: 613-615 and Figure 16.

- Figure 17: I'm not sure I understand the life mentioned in each subfigure, which ranges from 20 to 10,000 years. Is this the basic life for an individual 10-minute bin "j" from Equation 6, or the combined and modified life from Equation 8? The use of L10m,f and L10m,r in the Figure says the latter, but it feels like it is a graph of the former. Equation 8 implies a_ISO has a single fixed value and is applied to the combined L10; however, Figure 17 implies a_ISO is calculated for every 10-minute period from the main bearing temperature and dynamic equivalent load (and fixed contamination level and fatigue load limit) and applied to the basic L10 before being combined. Is this a correct understanding?

  Response: The authors appreciate the comment as it identified a poor definition of the a_{ISO} in Section 2. The $a_{ISO,j}$ is actually calculated for each 10-min j instance. And so is the modified rating life L_{10m} of the rear and front main bearing.

  Revised Section: Equation 8 has been updated to present $L_{10m,j}$ calculated for each 10-min j. The mapping of the L_{10m} continue to be as function of the environmental conditions.

  See lines: Equation 8

- Lines 491–492: Like section 5.5.2, a citation of Kenworthy (2024) would be appropriate here, as they came to the same conclusion.

  Response: Agreed. The reference to Kenworthy (2024) has been added. In addition, a reference to Quick (2025), a WES pre-print, has been added as it is also an appropriate reference.

  Revised Section: The discussion to the Figure 14 (previous Figure 16) has been reformulated and incorporated Kenworthy (2024) and Quick (2025) references.

  See lines: 587

- Line 496: Here L10,r is given as 315 years, while if I understand the Abstract and section 5.2.1 correctly it is 333 years. Shouldn't they be the same?

  Response: Agreed. The authors appreciate the attention from the reviewer. It has been an error from the authors in the documentation. The values have been updated in the Abstract and Sections 5.2.1 and 5.5.3, now are the same.

  Revised Section: Abstract and Sections 5.2.1 now have the value of $L_{10,r}$ equal to 566 years.

  See lines: 10

6 Discussion

- If it were me, I would integrate anything new in Section 6 into the main body of the article itself. It's an opportunity to shorten the article, as it feels much of what is described here has already been stated earlier, and there's an additional Conclusions section.

  Response: Agreed. The text and discussions previously contained in Section 6 (Discussion) but have included in Section 5 (Results) and Section 7 (Conclusion).

  Revised Section: The previous Section 6 (Discussion) has been removed. The important take-aways have been included in the Results and Conclusion.

- Line 502: Strictly speaking, I think this should state "...eight full strain gauge bridges...", shouldn't it?

  Response: Agreed.

  Revised Section: The suggested sentence has been added in Section 6.

  See lines: 691

- Lines 523–526: Like previous comments on Section 5.5.1, Abstract, and Conclusions, I believe these sentences are misleading. Among other reasons, stating "The stiffness of the gearbox mounting could lead..." alone is rather vague. What is meant here is "Assuming the gearbox is rigidly mounted could lead..."; however, as stated earlier, this is an usual assumption. It is more typical to assume the gearbox mounting has little or even no stiffness. As mentioned earlier, I would rather see these statements "flipped" in their comparative sense, with the resulting conclusion being that modeling of the gearbox stiffness had little impact on Peq or L10 (actual amount TBD).

  Response: Agreed.

  Revised Section: The discussion on the gearbox stiffness has been removed from the Abstract and Conclusion, being limited to the Section 5.5.1. With the statement "flipped" as suggested by the reviewer.

  See lines: 563-568

- Lines 530–534: The sentences here regarding the relative importance of TI to other factors seem to be in some ways contradictory and in other ways misleading. Both Kenworthy (2024) and the results in this manuscript indicate that main bearing temperature and grease cleanliness first and foremost, followed by shear, are much larger factors in main bearing rating life than the turbulence intensity. The reader would not get that sense right now.

  Response: Agreed. The paper pre-print Abstract, Section 5.5.2 and Conclusion were initially misleading the reader. The authors have reformulate to make sure that the thrust curve is the driver of the fatigue load in the locating main bearing. Whereas, at the rated wind speed (most damaging condition) both low turbulence and shear showed similar effect on the increased loads. And once the modified rating life L_{10m} is presented, temperature and grease cleanliness levels prevail.

  Revised Section: Abstract, Section 5.5.2 and Conclusion have been modified to incorporate the suggested reviewer feedback, while still arguing that low turbulence had the similar effect as low shear in the locating rear main bearing.

  See lines:20-22, 583-589 and Figure 15.

7 Conclusion

- Line 558: I recommend this be changed to "...has a longer life as the shear exponent increases..."

  Response: Agreed.

  Revised Section: The suggested sentence has been added in Section 6.

  See lines: 712

- Line 560: As mentioned earlier, the statement "... the rear main bearing, at rated wind speed, has higher loads for lower turbulence intensities" seems to have mis-placed emphasis. It is extremely difficult to see this in Figure 16, when in comparison the mean wind speed has a far, far greater effect. I am not able to tell whether, for a given wind speed, if a change in TI or shear exponent has a greater effect.

  Response: The authors hopefully have managed to better discuss the effect of the thrust curve, Quick (2025), and the turbulence effect in the lifetime of the locating main bearing as shown in Figure 15. Once the discussion of the results has been reformulated, the authors seek only to describe the mapping of load measurement from 2016 to 2024 (inclusive), which identified a effect of the turbulence intensity as high as of the shear. The first driver (turbulence intensity) is in agreement with the HIPERWIND 5.4 report, whereas the second driver (shear) in in agreement with Kenworthy (2024).

  Revised Section: As previously mentioned, Abstract, Section 5.5.2 and Conclusion have been modified to incorporate the suggested reviewer feedback.

- Line 560: The statement "Neglecting the stiffness of the gearbox mount renders unrealistically high Peq, but having the stiffness values within realistic ranges results in little influence on the lifetime" hearkens back to Section 5.5.1, but I believe it uses wording opposite to Figure 15b. From Figure 15b, I would write this statement that "Assuming a rigid gearbox mount renders unrealistically high Peq..." or "Neglecting the stiffness of the gearbox mount has a minimal impact on Peq". See previous comments on Section 5.5.1 and Figure 15b. Like the Abstract, it's worth considering if this point is even important enough to mention in the Conclusion. It might be deleted without losing anything, as it's really a sensitivity study like downsampling the SCADA rate which is not mentioned in the Conclusions. I leave it to the authors to decide.

  Response: Agreed.

  Revised Section: The authors have removed such text from the Abstract and Conclusion and reformulated the discussion in Section 5.5.1.

  See lines: 563-568

- Line 562: Although this may be true, is there a reference that can be cited that life corrections have been validated for other bearings (smaller and/or oil lubricated)? Such a statement would actually be beneficial earlier in the manuscript, rather than only here.

  Response: Agreed. The authors appreciate the feedback as it supported the theoretical background of the paper to become more robust.

  Revised Section: A reference to the "Recalibrated Equations for Determining the Effect of Oil Filtration on Rolling Bearing Life" report by NASA, Needelman and Zaretsky (2014), has been added to Section 2.2 and Conclusion. The document reports a review of several relevant references investigating, among other topics, the impact of the lubricant cleanliness in the bearings lifetime "Life factor LF" (pitch diameter of reference is 100 mm), such as the impact of particle contamination according to the particle size in oil filtration.

  See lines: 149 and 720-722

Minor grammatical comments

Response: We appreciated the careful reading and detailed correction on the grammatical errors. Thank you for your patience and time.

Revised Section: All comments below have been incorporated as suggested. For the sake of conciseness, they will not be replied individually, but their suggested lines are still coherent if checks are to be made. Further small grammatical corrections have been made and citation style changed in the response manuscript.

- Line 5: Rather than "minimally intrusive strain gauge at blade and tower" I believe simply "tower and blade root strain gauge bridges" is clearer.

- Line 26: I believe the preferred citation style is here "... global benchmark reports (IEA and NEA, 2020; IRENA, 2024)." Similar for line 29 "... the foundations (Ziegler et al. 2018; IEC-TS-61400-28, 2020)."
- Line 42: Use plural "reported failures" here.
- Line 45: Use citation style "(Santos et al., 2024)" here. I recommend reviewing citation style throughout. Maybe the WES editors will take care of this themselves.
- Line 86: Should be "number of cycles" here.
- Line 102: I'm not sure "reasoning" is correct here, I believe the meaning is "meaning" as used later in line 104.
- Line 113: Italicize P, X, and Y here in the text.
- Line 139: I'm not sure I understand the meaning of "Benefiting from instances statistics...". Similarly for line 159.
- Line 146: A space is needed "... different. Similarly, Dimitrov and Gocmen (2022) show..."
- Line 194: Does the V25 have a S355 steel tower as stated in line 79, or only "assumed" to have a S355 steel tower as stated here?
- Line 197: Here and elsewhere, I believe "L10,m" should be "L10m".
- Line 262: Here "... time steps,NlaggedFNN Dimitrov and Gocmen (2022)..." seems a little garbled. Is "Nlagged" a variable?
- Line 270: DLC does not need to be redefined here, as it was already done in Line 77. Similar for other instances of "design load cases (DLC)" after this point.
- Line 324: There is a double period in this line.
- Line 433: There is a double-space here.
- Line 439: Instead of "is incremental", I believe "incrementally increases" makes more sense here.
- Line 541: Should be "continually calibrated".

3 Response to Reviewer 2

This paper presents an interesting approach to continuous lifetime monitoring of wind turbine towers and main bearings using strain gauge calibration and virtual load sensors over nearly 10 years of data. The methodology is comprehensive and the long-term dataset is valuable. However, several clarifications and corrections are needed before publication, as outlined below.

Response: The authors greatly appreciate the critical feedback. The results related to the virtual load sensors have been improved by incorporating the suggestions given by the Reviewer 2. Similarly for the general comments.

Revised Section: As previously mentioned to the Reviewer 1, an effort has been made to shorten the paper, and make the methodology more robust, specially, for topics related to the tower bottom virtual load sensor.

4 Comments and suggestions:

- The paper is quite long as another reviewer has also noted. Consider shortening by consolidating or removing redundant material. Some sections could be more concise.

  Response: Agreed. This feedback has been transparent and coherent to the Reviewer 1. The authors have made an effort to shorten the paper length.

  Revised Section: Figures 14-18 (Figures 12-16 in the reviewed paper) have been increased. The manuscript has been shortened by two pages while preserving all relevant findings

- The paper switches inconsistently between “nearly 10 years,” “9 years,” and “7.5 years” when describing different analyses. A clear timeline figure would help readers follow which period is being discussed in each section.

  Response: Agreed. The authors appreciated the attention given by the Reviewer 2 to this matter. The authors have not been consistent in the pre-print document in terms of a clear timeline.

  Revised Section: Instead of a timeline figure as suggested, which would take significant space, the authors have decided to be coherent along the main text. Now the mentioning to 9 and 7.5 years have been removed. The load measurement campaign has been presented to be carried out from 2016 to 2024 (inclusive) along the different sections of the paper. With the exception of to the deployment of virtual load sensor, which neglected a initial 35 Hz dataset as explained in the Section 5.4, and had a final timeline from June 2017 to 2024 (inclusive). The phrase “nearly 10 years”, instead of ”2016 to 2024 (inclusive)”, is used only in the Abstract and Conclusion to emphasize the long-term reliability of the strain gauges and the lifetime counting.

  See lines: ”2016 to 2024 (inclusive)” in line 179, Figure 5, Figure 6, Table 2, Figure 12, Figure 14, Figure 16. ”June 2017 to 2024 (inclusive)” in line 490 and Figure 9.

- The gearbox mounting stiffness of 20×10^6 N/m is from literature for different turbines. The sensitivity analysis shows this can cause 60% error in P_{eq}. How representative is this value for your specific drivetrain? How could this be validated in practice?

  Response: The authors appreciate the discussion. As pointed by the Reviewer 1, the pre-print draft was misleading when discussing the results from the sensitivity analysis for the gearbox mounting stiffness. The adjusted discussion aimed to emphasize the the exact value of the mounting is not as relevant as long as it is not model as a rigid support, but instead, as flexible with values close to the literature. Validation of such results could be performed by the application of testing loads in the torque arm mounting spring, but they are out of the scope of this paper.

  Revised Section: As suggested by the Reviewer 1, the discussion on the gearbox mounting stiffness has been reformulated in order to be more clear.

  See lines: 563-568

- The hyperparameter tuning used only 5 hours of data compared to 160 hours for training. Why do the authors use such a small amount? This seems inconsistent.

  Response: Agreed. The value documented int the pre-print was not correct. The hyperparameters for the tower bottom virtual load sensors have been tuned with 10 hours, whereas 5 hours was used for the tuning of the blade root virtual load sensors pursued in a past conference article (Faria et al., 2025). The 10 hours subset is still not as large but one should considered that 3 seeds have been used during the Random Search optimization framework, which increases the robustness of the tuned values.

  Revised Section: The value documented in Section 4.3 has been updated to 10 hours and a mention to the 3 seeds is also made.

  See lines: 313-314

- You trained on 160 hours but validated on 160 hours from 2019. How was the validation set selected? Same k-means or random?

  Response: Yes. Indeed, this information was missing from the pre-print version. Thank you for the carefull reading.

  Revised Section: The validation set has also been selected using K-means, as added in Section 5.3.

  See lines: 450

- There is a fundamental clarity issue with the lifetime calculations in Section 5.2.1 and Figure 7. The accumulated damage values shown in the figure do not align with the stated lifetimes of 166 years for the front main bearing and 333 years for the rear main bearing. The same issue appears for the tower bottom lifetime. Please verify and clarify these numbers.

Response: Agreed. The authors appreciate the attention of both Reviewer 1 and 2 to the wrong documented values-

Revised Section: The tower bottom fatigue lifetime is actually 2952 years, whereas the front and rear main bearings lifetime is 282 and 566 years respectively. The correction has been applied to the Abstract and Sections 5.2.1 and 5.5.3.

See lines:10 and 410-411

- Figure 12b shows the correction factor varies across years for different inputs. Using an average value could introduce bias depending on which year dominates. Did the authors check if this correlates with annual wind statistics?

  Response: The pre-print was misleading the reader by suggesting that the virtual load sensors was corrected solely by the average slope, when actually, it is corrected by the maximum/minimum, standard deviation and average of the slope. The experimental slope correction tries to incorporate such biases by using not only the average, but also the standard deviation and maximum/minimum areas in Figure 11 (previous Figure 13). In this way, one could pick a year by chance and still have a uncertainty quantification. Regardless, the authors agreed that the driver of this bias could be the annual wind statistics. Such effect has not been validated, but the discussion suggested by the reviewer has been added.

  Revised Section: Text related to the Figures 10 and 11 in Section 5.4.1 have shortly incorporate the suggested discussion of the reviewer. And future research should be guided by the proposed discussion.

  See lines: 511-512

- Figure 11 shows all virtual sensors systematically underpredict tower damage. The proposed correction method needs 6 months to 1 year of real measurements for calibration. This limits the benefit, and you still need substantial measurements. What is the minimum period needed for reliable correction?

  Response: The authors agreed that this would be a interesting exercise and should motivate following research.

  Revised Section: Section 6 (Conclusion) has incorporated the suggestion from the Reviewer. The authors have a great interest in continuing the research to investigate the needed load measurement periods and their associated model uncertainty for the slope correction.

  See lines: 704-705

- LSTM with strain inputs (no accelerometer) performed worse than simpler FNN. Needs more explanation than just "LSTM cannot attenuate 1P, 2P, 3P contributions." Why would temporal modeling perform worse with these periodic signals?

  Response: The authors agreed that the pre-print did not contain any further explanation commenting the performance of the LSTM without nacelle accelerometer. A discussion has been added with a possible explanation.

  Revised Section: In Section 5.3, the following text has been added "The LSTM added unrealistic oscillations in the time-series estimate with larger 1P, 2P, and 3P frequency contributions and underpredicted the 1^{st} FA frequency contribution, most likely due to poor model coupling of the blade strain gauges and azimuth angle φ inputs." The claim is that the sin/cos fed signals of the azimuth angle φ were not been properly coupled by the model to incorporate the turbine fore-aft motion resultant of the combination of the individual blade root strain gauges (bending moments) as function of the azimuth angle (thrust curve).

  See lines: 456-459

- Low turbulence increasing bearing loads at rated wind speed is interesting but not sufficiently explained. The authors cite HIPERWIND D5.4 but no intuition provided. Could this be because the control system switches between modes frequently with turbulent inflow, leading to peak thrust? (see https://doi.org/10.1115/1.4041996)

Response: The authors agreed that the effect of the turbulence has not been sufficiently explained. It is claimed by the authors that the higher fatigue loads observed for low turbulence is driven by the peak of the thrust curve. The suggested reasoning given by the reviewer is valid, but the authors believe that following the claim of "control system switches between modes frequently with turbulent inflow", higher turbulence should then drive higher loads, which is not observed in this paper.

Revised Section: Figure 15 has been added to support further discussion on the claim that lower turbulence should lead higher fatigue loads in the locating main bearing.

See lines: 581-608, Equation 20 and Figure 15

Continuous lifetime monitoring technique for structural components and main bearings in wind turbines based on measured strain and virtual load sensors

Bruno Rodrigues Faria [1], Nikolay Dimitrov [1], Nikhil Sudhakaran [1], Matthias Stammler [1,2], Athanasios Kolios [1], W.Dheelibun Remigius[3], Xiaodong Zhang[4], and Asger Bech Abrahamsen [1]

[1]DTU Wind and Energy Systems, Technical University of Denmark, 4000 Roskilde, Denmark
[2]Large Bearing Laboratory, Fraunhofer Institute for Wind Energy Systems IWES, 21029 Hamburg, Germany
[3]Shell India Markets Private Limited, 562149 Bengaluru, India
[4]Science and Technology Institute, China Three Gorges Corporation, 101100 Beijing, China

Correspondence: Bruno Rodrigues Faria (brofa@dtu.dk)

Abstract.

Decisions on the lifetime extension of wind turbines require evaluating the remaining useful life of major load-carrying components by making a comparison to the design lifetime. This work focuses on the lifetime assessment of two fundamentally different components: a structural component in the form of the tower and rotating components in the form of the main bearings. A method is presented that combines high-frequency SCADA, accelerometers, ~~minimally intrusive strain gauge at blade and tower~~tower bottom and blade root strain gauge bridges, and limited design information for continued estimates of the component loads and their subsequent fatigue damage accumulations. The work is applied to a highly instrumented DTU research turbine, a Vestas V52 model, where strain gauges in the blade root and in the tower bottom are calibrated for nearly 10 years using continual calibration methods without the need for operator input. The lifetime estimates of the tower bottom and front and rear main bearings were found to be ~~1770 yearsand 166-333~~ 2952 years, 282 years and 566 years, respectively, reflecting the low average wind speed of the turbine site compared to the wind turbine design wind class IA. Secondly, it was investigated whether virtual load sensors can replace tower strain gauges~~and if one can use only uptower sensors for lifetime evaluation~~. Consistent tower bottom strain signal estimate and long-term damage accumulation were achieved with $\pm 5\%$ lifetime variability once SCADA, nacelle accelerometers, and blade root strain gauges were combined for the deployment of a long short-term memory (LSTM) neural network. A systematic underprediction of the accumulated damage of the tower bottom was observed for the virtual load sensors with a reduced set of inputs, and a correction method was proposed. Finally, the impact of environmental conditions, including turbulence intensity and shear exponent of the incoming wind, on the main bearing lifetime was investigated ~~using 10 years of~~ based on load measurements. A simple drivetrain thermal model was used to evaluate the modified lifetime L_{10m} of the main bearings~~, depending on the measured ambient temperature and the grease cleanliness assumptions. Higher fatigue loads are observed on the main bearings~~. Fatigue loads in the locating main bearing are driven by the peak of the turbine thrust curve with higher loads observed at rated wind ~~speeds with low turbulence intensity and low shear. Changes of ± 5 °C in the ambient temperature around 15 °C caused a 10-year difference in the operational life~~

~~of the main bearings~~ speed. An effect of longer main bearing lifetime with higher turbulence intensity was observed at rated wind speed ~~. It was also found that the specification of the gearbox mounting stiffness can lead to a 60% overprediction of the main bearing loads.~~ and can be explained by the turbulence averaging of the thrust loads.

1 Introduction

The extension of the lifetime of wind turbines provides an opportunity to decrease the levelized cost of the electricity produced by wind turbines, which is not only competitive, but in many cases the cheapest electricity source according to evaluations of multiple global benchmark reports ~~such as~~ (IEA and NEA, 2020; IRENA, 2024). At the same time, lifetime extension could decrease the global warming potential ($CO_{2,eq}$ / kWh) emitted during the entire life cycle of a wind turbine (UNECE, 2022).

Lifetime extension of wind turbines is ~~then strongly~~ often dictated by reliable technical evaluations of the consumed and of the remaining useful lifetime of structural components such as the tower and the foundations ~~as described by~~ (Ziegler et al., 2018; IEC-TS-61400-28, 2020). Such large components are site-specific and little ~~to no~~ experience can be found in replacement of those during the lifetime and beyond, as this would hinder the profitability of a wind farm. Similarly, having unexpected and several load-carrying components failing would require long-lasting replacements that would increase the operational expenditure (OPEX) of a wind farm and reduce its revenue. That is the case with the main bearings. OPEX estimates should be based on the probability of failure of such components combined to their availability in the spare market.

As a ~~failure in the main bearing means a failure in turbine operation~~main bearing replacement incurs significant costs and turbine downtime, this decision should be made with high levels of certainty. A main bearing failure results in high replacement costs, between $225,000 and $400,000, loss of revenue due to production interruption, and its failure is one of the main reasons for the increase in OPEX, especially in onshore wind turbines of 2 to 6 MW in size according to Pulikollu et al. (2024). Although main bearings are known to have multiple failure modes, as examined by Hart et al. (2020), including abrasive and adhesive wear and fretting, this work considers lifetime consumption as the fatigue life consumption of the main bearing. This is due to the leading role of rolling contact fatigue (RCF) which can not yet be ruled out with respect to historical replacement data of the main bearings. Hart et al. (2023) carried a large review of historical data on the damage and failure of the main bearing and identified that for a large share (80%) of the reported ~~failure~~failures, spalling was present, which could be a consequence of both subsurface- and surface-initiated RCF.

In this context, the end goal of a well-designed structural health monitoring (SHM) campaign is to have the most comprehensive and reliable wind turbine monitoring and lifetime estimation with the least amount of instrumentation ~~Santos et al. (2022)~~ (Santos et al., 2022). And using strain gauges often results in one key drawback: compromised long-term reliability. There has been a literature gap on the possibility of calibrating strain gauges for many years, with some ~~studies to mention Pacheco et al. (2024)~~ investigations to mention (Pacheco et al., 2024). So, the question of how to extrapolate the lifetime of components based on limited recordings has been of interest and widely investigated (Loraux and Brühwiler, 2016; Hübler and Rolfes, 2022; Sadeghi et al., 2024; de N Santos et al., 2024). However, no consensus has yet been reached on the methods or uncertainties related to those methods. In this context, data-driven methods ~~Dimitrov and Göçmen (2022); Pimenta et al. (2024)~~ (Dimitrov and Göçmen, 2022; Pin

deployed as long-term virtual load sensors could yield several advantages by replacing real sensors and reducing the amount of instrumentation needed, being able to describe complex mathematical correlations, with no real physical understanding of the system.

Considering the challenges and gaps identified, this work aims to ~~maximize coverage using~~ use existing onboard sensors and limited non-invasive hardware additions, to evaluate the lifetime of structural and rotating component simultaneously. ~~Based on this objective, the~~ The following research questions guided the methodology and subsequent analysis.

- Is it possible to continuously and reliably count the lifetime of a tower and a four-point configuration main bearing without blade design information and having ~~in hands~~ access to SCADA, blade root, and tower bottom strain gauges, while meeting ISO-281 (2007) and IEC 61400-1 (2019) standards?
- What degree of accuracy could be achieved by a tower bottom virtual load sensor based on measurements in the nacelle?
- What are the environmental and operation conditions (EOC) which have strongest impact on the basic and modified rating lifetime of the main bearing (L_{10} and L_{10m}, respectively), based on analysis of a long-term measured dataset?

The remaining sections of this paper are organized as follows. Section 2 provides an overview of the theoretical background relevant to this work, including the assumptions behind the tower fatigue lifetime and the main bearing lifetime, as well as the concept of virtual load sensors applied in this study. Section 3 describes the wind turbine and the environmental measurement campaign used for data collection. Section 4 details the proposed methodology for the calibration of the strain gauge and the lifetime of the tower and main bearing based on load measurements and virtual load sensors. The results obtained are presented in Section 5, ~~followed by a discussion in Section **??**, where the findings are~~ including a discussion of the findings compared to the relevant literature, and key correlations are analyzed. Section 6 concludes the paper by summarizing the main insights and learnings from this work.

2 Theoretical background

~~Behind the key assumptions of this work, mentioned in the introduction and shown in Figure 2, some require further explanation.~~ The concept of tower fatigue and main bearing lifetime is assumed as derived in standards used for design and certification. The concept of virtual load sensors can also be very broad. In this work, we will focus on time-series and data-driven virtual load sensors that could be used to replace tower bottom strain gauges ~~at a wind farm level and keep instrumentation in the nacelle~~in case of sensor failure. More details of each subject are described in the following subsections ~~.~~ and with Figure 2 providing an overview of the methodology.

2.1 Tower fatigue lifetime

The lifetime is estimated as described by IEC 61400-1 (2019), considering the Design Load Cases (DLCs) 1.2 (Power production), 3.1 (Start-up) and 4.1 (Normal Shutdown). More details on how to classify these operational conditions based on

~~10-min~~ 10 min SCADA can be found in Faria et al. (2024). On the material side, the ~~DTU research tower~~ tower of DTU research V52 turbine is made of structural steel S355, which is often used in large components and harsh environmental conditions. In this work, the fatigue assessment of critical welds assumes that the component has inherent defects in the welded joints and thus does not model crack initiation or growth.

The first step is to convert a measured tower bending strain ϵ [μmm/mm] to bending stress σ [Pa] as shown by Hooke's rule $\sigma = E \cdot \epsilon$. The bending stress can be translated into the bending moment M assuming the tower is a Euler-Bernoulli beam.

$$\sigma = \frac{M \cdot c}{I} \tag{1}$$

where I [m^4] is the area moment of inertia and c [m] is the radius, in the case of a circular cross section. To evaluate fatigue, the stress time series is converted to stress ranges $\Delta\sigma_i$ and ~~umber~~ number of cycles n_i using the rainflow counting technique, as described by ASTM E1049-85 (2017). The tower bottom in this work is evaluated using the category of the stress cycle (SN) curve category "D", for butt-weld in air as suggested by DNVGL-RP-C203 (2016), which translates $\Delta\sigma_i$ into a maximum amount of cycle to failure $N_{max,i}$. Finally, fatigue accumulation, in other words, fatigue lifetime is assumed to be linear, according to Palmgren and Miner (1945), which is valid for any time window, from high-frequency to ~~10-min~~ 10 min instances to lifetime.

$$D_T = \sum_j^{N_j} D_{T,j} = \sum_j^{N_j} \sum_i^{Ni} \frac{n_i}{N_{max,i}} = \sum_j^{N_j} \sum_i^{N_i} \frac{n_i \cdot (\Delta\sigma_i)^{m_i}}{K_i} \tag{2}$$

where D_T is the tower accumulated fatigue damage (failure at unity), $D_{T,j}$ is the accumulated fatigue damage of the ~~10-minute~~ 10 min instance, m_i is the exponent of the SN curve, K_i is the intercept of the SN curve on the y-axis, N_j is the number of 10 min instances and N_i is the number of cycles in a given instance.

The ~~exponential~~ non-linear nature of fatigue can be observed ~~and its non-linearity due to~~ from the SN curve having different m_i and K_i dependent on the two regions of the SN curve where the cycle could be placed. In order to facilitate the evaluation of virtual load sensor during training and validation, instead of comparing D_T, Damage Equivalent Loads (DELs) are often used and can be explained as single-frequency sinusoidal loads that would inflict the same damage as the initial load variable in time, as in

$$DEL = \left(\sum_i^{N_i} \frac{n_i \cdot \Delta\sigma_i^m}{N_{ref}} \right)^{1/m} \tag{3}$$

where m is assumed to be 4, which is an average between DNV "D" curve values of m_i equal to 3 and 5 and log_{K_i} equal to 12.164 and 15.606, respectively, transitioning at N_{max} equal to 10^7 cycles. The N_{ref} is a normalization factor and is arbitrarily assumed to be 10^7 cycles, since DEL has no absolute ~~reasoning~~meaning.

~~However, for~~ For the estimation of the consumed and remaining useful lifetime of a tower, and the deployment of the virtual load sensor ~~in the long-period~~over long periods, DEL has no absolute meaning and its uncertainty underestimates the uncertainty of the useful life of the component and, therefore, D_T should be prioritized. More discussion is present in Section 5.3.

2.2 Main bearing fatigue lifetime

The lifetime of a rotating component, such as a main bearing, can be significantly more complex to model than the tower lifetime. In this work, the formulations from ISO-281 (2007) are followed, which also defines the linear accumulation of damage as proposed by Palmgren, using the same DLCs as for the tower. As mentioned, rolling contact fatigue is not the only damage mode of the main bearings, but the inclusion of additional mechanisms is not in the scope of the present work.

The radial F_r [N] and axial F_a [N] load acting on the main bearings are combined into

$$P = X \cdot F_r + Y \cdot F_a N \tag{4}$$

where ~~P~~ P [N] is the dynamic load, ~~X and Y~~ X and Y are functions of the load ratio F_a/F_r and the limiting value e, as often provided by the bearing manufacturer. The time-varying P can be replaced by a constant equivalent load P_{eq} that would have the same deterioration at its given operational rotation speed, similar to the defined DEL, without involving any counting method.

$$P_{eq} = \left(\frac{\sum P_i^p \cdot \omega_i}{\sum \omega_i} \right)^{1/p} \tag{5}$$

where P_i [N] is the dynamic load, p is the exponent dictated by the type of rolling body (e.g. ball or roller) as provided by ISO-281 (2007), and ω_i [rpm] is the rotational speed of the main bearing at the instantaneous i timestamp.

Then, the basic rating life L_{10} is defined as the 90% survival time of a given population of main bearings under similar operational conditions. In other words, 10% of the bearings would fail.

$$L_{10,j} = 10^6 \left(\frac{C_d}{P_{eq}} \right)^p \text{[revolutions]} \qquad L_{10,j} = \frac{10^6}{60 \cdot \omega \cdot 8760} \left(\frac{C_d}{P_{eq}} \right)^p \text{[years]} \qquad L_{10} = \frac{1}{\sum \phi_j / L_{10,j}} \text{[years]} \tag{6}$$

where L_{10} is the basic rating life overall while $L_{10,j}$ is the basic rating in a given ~~10-minute~~ 10 min instance j. If all instances have the same ~~10-min~~10 min, ϕ_j is the inverse of the number of instances. C_d [N] is the dynamic load rating, ~~p is the exponent function of the rolling body type (e.g. ball or roller) as provided by ISO-281 (2007),~~ P_{eq} [N] is the ~~dynamic equivalent load~~ equivalent dynamic load, and ω [rpm] is the rotational speed of the main bearing within a ~~10-min~~ 10 min instance. Once L_{10} is calculated as the number of hours to failure in each instance, one can describe a main bearing damage accumulation, similar to the damage accumulation in the tower, as in

$$D_B = \sum_j^{N_j} D_{B,j} = \frac{t_{operation}}{L_{10}} \tag{7}$$

where D_B is the accumulated fatigue damage of the main bearing (failure at unity), $D_{B,j}$ is the accumulated fatigue damage of the ~~10-minute~~ 10 min instance, and $t_{operation}$ is the evaluated time of operation in years.

~~In order to incorporate a more realistic effect of operating conditions on the main bearing, a~~ To account for operating conditions more realistically, the life modification factor ~~a_{ISO} should be evaluated . The latter considers that the lubricant will be exposed to different operating temperatures and its value will be affected by the level of~~ a_{ISO} (ISO-281, 2007) is

evaluated for the main bearing. This factor accounts for variations in operating temperature and lubricant condition, and is influenced by grease cleanliness, ~~the~~ operating viscosity (~~function of temperature), the~~ temperature dependent), rolling element type, bearing fatigue limit, and external loads ~~. The complete formulation can be found in ISO-281 (2007). The~~ (Needelman and Zaretsky, 2014). The modified rating life ~~L_{10m} of a~~ L_{10m} of the main bearing is then calculated using

$$L_{10m\,10m,j} = L_{10\,10,j} \cdot a_{\mathrm{ISO\,ISO},j} \tag{8}$$

where $a_{\mathrm{ISO},j}$ is the modification factor calculated for each 10 min instance j. In this work, a drivetrain thermal model is used to allow the estimation of $a_{\mathrm{ISO},j}$, as shown in Section 4.2. The $L_{10m,j}$ can be accumulated as given in Equation 6 for L_{10}.

2.3 Virtual load sensors

In this work, virtual load sensors are seen as an opportunity to replace physical sensors to estimate tower bottom bending moments and long-term fatigue lifetime~~, keeping the necessary measuring in the nacelle~~. In the literature, several efforts have been made in the regard of data-driven (machine learning) models for lifetime predictions of components.

Benefiting from ~~instances statistics and~~ 10 min instance statistics (e.g. mean and standard deviation) and more available SCADA accelerometers, efforts were made to estimate target statistics such as damage equivalent loads (DELs) or damage to the main bearing. Mehlan et al. (2023) estimates aerodynamic hub loads and tracked bearing fatigue damage using a digital-twin based virtual sensing combining SCADA and condition monitoring. For support structures, de N Santos et al. (2024) estimates the fatigue lifetime based on different combinations of SCADA levels, highlighting the improvement in performance using reliable nacelle accelerometers, with a novel population-based approach for wind farm extrapolation. Focusing on time extrapolation, Hübler and Rolfes (2022) focuses on different methodologies to extrapolate damage in time and their estimated uncertainty. On the other hand, when the time series signal is the target output, the model selection and training process are quite different. Complementary, Dimitrov and Göçmen (2022) shows how machine learning time series models (e.g. LSTM) can act as virtual sensors for blade root bending moment trained on aeroelastic simulations. ~~More recent efforts extend virtual sensing to floating turbines.~~ Gräfe et al. (2024) trained neural networks on simulated floater motions and LIDAR-derived wind to ~~reconstruct fairlead tensions and DELs~~estimate tension and DEL of mooring lines.

The same data-driven models applied by Dimitrov and Göçmen (2022) are selected to be used in this work on the DTU research V52 turbine dataset, all derivatives of neural network architectures. This work contribution to virtual load sensor methods lies in the validation of a model that should accurately replicate both: (1) the time series of tower bottom bending moments and (2) the fatigue loads of the tower and main bearings in the long term. (1) The first can have its performance quantified by ~~feeding~~ using the virtual load sensor as a thrust estimate to calculate the lifetime consumption of the main bearings. (2) The latter includes the 3 most damaging operational conditions for the tower as described in Pacheco et al. (2024); Faria et al. (2024): power production DLC 1.2, start-up DLC 3.1, and shutdown DLC 4.1, all in a single model.

3 Measurements

In this work, SCADA data and measurements from nearly 10 years are analyzed from ~~February~~ 2016 to ~~December~~ 2024 (inclusive) at Risø, Denmark. The environmental conditions are analyzed out of ~~10-min~~ 10 min instances statistics from a met mast about 100 m east of the DTU research V52 turbine. In addition to the mean wind speed U_{hub} at the hub height of z_{hub} = 44 m, the turbulence intensity is calculated as $TI = \sigma_U/U$, where σ_U is the standard deviation of the wind speed. Moreover, vertical shear is modeled considering the normal wind profile model IEC 61400-1 (2019) given by the power law equation $U(z) = U_{hub}(z/z_{hub})^{\alpha}$, where z is the height and α is the shear exponent. The latter is estimated as the best fitting factor out of five different cup anemometers measuring heights (at 18, 31, 44, 57 and 70 m) for each ~~10-min~~ 10 min instance. No shadow correction was performed for the mast tower. In general, it is possible to observe that the Risø site has fairly low wind and constant ~~conditions~~wind flow conditions over the years. The yearly wind speed U_{hub} ~~, estimated as a Weibull function in the graph on the left,~~ has a mean ~~below 6~~ value of 5.6 m/s. The site reference turbulence I_{ref} calculated as $I_{ref} = \sigma_U/(0.75U_{hub} + 5.6)$, has a mean value around 0.08 (closer to IEC class C) and the shear exponent α of 0.22. The prevailing wind direction falls within the southwest quadrant across all years. The DTU research V52 turbine is a Vestas 850 kW onshore wind turbine class IA with a rotor diameter of 52 m and a hub height of 44 m, with a active pitch and rotor speed control. SCADA and SHM measurements are available from February 2016 to December 2024, as are statistics and high-frequency data. The turbine has a rated wind speed of approximately 14 m/s. Figure 1 represents the turbine schematic and part of its instrumentation, highlighting the two measurement setups present in the tower bottom (a–a) and blade root (b–b). SCADA includes rotor speed ω, pitch angle θ, yaw angle γ, azimuth angle φ, and power. All of the bending moments shown are obtained from full Wheatstone ~~bridge~~ bridges installed in the components. This configuration has a couple of important advantages as higher signal-to-noise ratio, is temperature independent and optimized for measuring bending stress ~~, see Hoffmann (1989)~~(Hoffmann, 1989). A problem in the quality of the ~~measured azimuth angle γ, carried out~~ azimuth angle φ measured by a proximity sensor on the shaft flange, was identified before 2018 and after 2022, probably due to surface dirt. A correction was applied to all the raw signal to account for that, by combining the controller rotor speed signal with the measured azimuth to have a more reliable estimate of the azimuth angle (please refer to Appendix A). Taking into account Figure 1~~(c_1)~~c_1, the tower bottom fore-aft bending moment $M_{fore-aft}$ (downwind) can be calculated as in Equation 9.

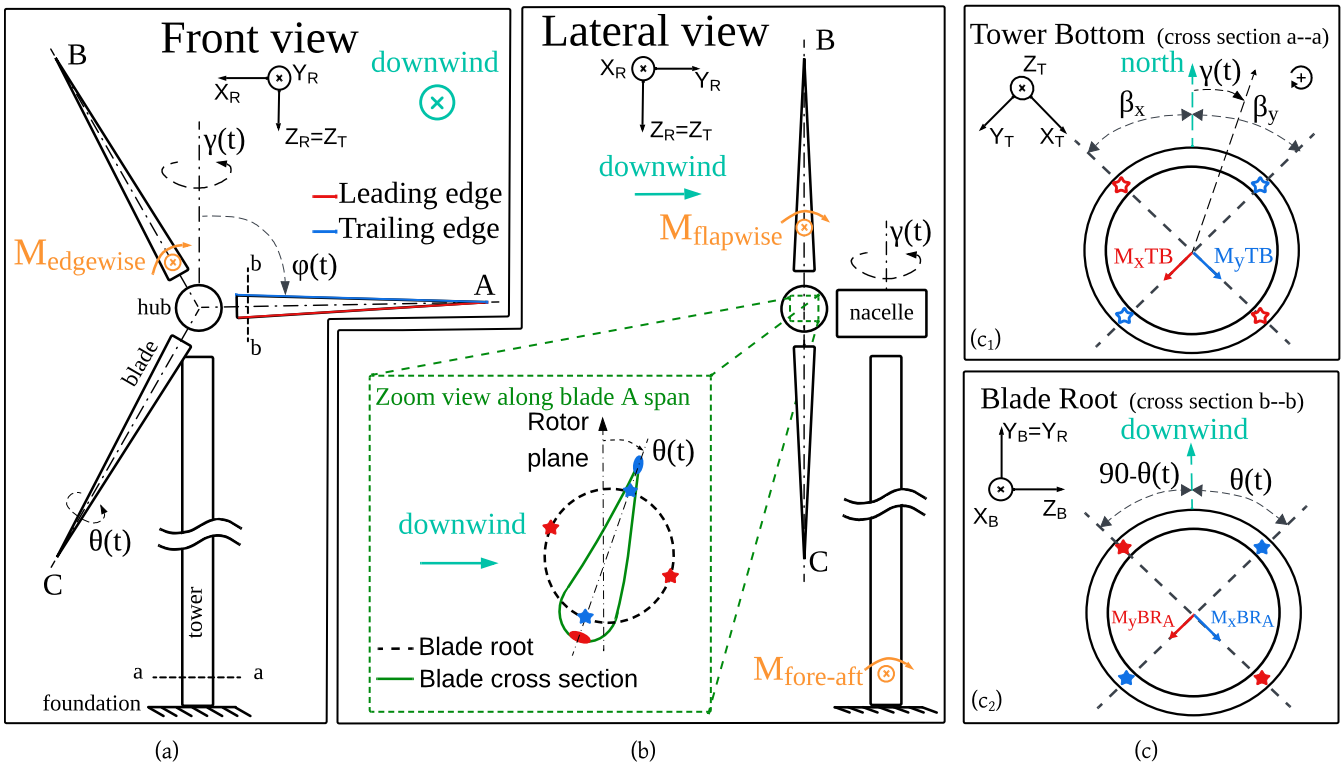

Figure 1. Schematic of an onshore wind turbine to represent the DTU research V52 turbine parameters and measurements. (a) Front view shows the rotor coordinate system XYZ_R which ~~moves~~ rotates with the yaw angle $\gamma(t)$ around Z_T and is facing the wind direction. The azimuth angle $\varphi(t)$ of blade A and pitch angle $\theta(t)$ are also shown. The $M_{edgewise}$ represents the edgewise (in-plane) blade root bending moment. (b) In the lateral view, the flapwise (out-of-plane) rotor bending moment $M_{flapwise}$ and the tower bottom fore-aft bending moment $M_{fore-aft}$ are shown. The $\theta(t)$ angle is the controller-defined blade root angle between the rotor plane and the chord line of the blade, as shown in the zoom view (green dashed box). (c_1) Tower bottom cross section (a–a) in the global/tower coordinate system (time-invariant) XYZ_T is determined. $M_{fore-aft}$ is dependent on $\gamma(t)$, as a composition of the measured tower bottom bending moments $MxTB$ and $MyTB$, which are obtained from strain gauges (stars) installed at the angles $-\beta_x$ and β_y respectively. (c_2) Blade root A cross section (same setup for blades B and C) shown in the blade coordinate system XYZ_B, which rotates with $\varphi(t)$ in respect to Y_R. Both measured blade root bending moments M_xBR_A and M_yBR_A shall be converted into $M_{flapwise}$ and $M_{edgewise}$ as function of the pitch angle $\theta(t)$.

$$M_{fore-aft}(t) = \frac{(-M_xTB(t)\cdot\sin(\beta_y-\gamma(t)) + M_yTB(t)\cdot\sin(\beta_x+\gamma(t)))}{\sin(\beta_x+\beta_y)} \tag{9}$$

in which the denominator factor is imposed because the two tower bottom bending moments are not perpendicular. Similarly, considering the measurement setup shown in Figure 1~~(c_2)~~c_2, the blade root flapwise $M_{flapwise}$ (out-of-plane) and edgewise

$M_{edgewise}$ (in-plane) bending moments can be calculated individually for blades A,B and C.

$$M_{flapwise,(A,B,C)}(t) = M_x BR_{(A,B,C)}(t) \cdot \cos(\theta(t)) - M_y BR_{(A,B,C)}(t) \cdot \sin(\theta(t)) \quad (10)$$

$$M_{edgewise,(A,B,C)}(t) = M_x BR_{(A,B,C)}(t) \cdot \sin(\theta(t)) + M_y BR_{(A,B,C)}(t) \cdot \cos(\theta(t)) \quad (11)$$

4 Methodology

Figure 2 shows the inputs and assumptions taken into account to investigate the research questions. From high-frequency turbine measurements to tower (structural component) D_T and main bearings (rotating component) D_B accumulation of fatigue damage over time. The orange boxes include the continual calibration of the strain gauges and the operations to translate the strain measurements of the tower and the blade to the tower bottom bending moment $M_{fore-aft}$, and the axial F_a and radial F_r main bearing loads. The standards shown (DNVGL-RP-C203, 2016; IEC 61400-1, 2019; ISO-281, 2007) provide the methods for the fatigue lifetime evaluations of each component, as explained in Section 2. The DTU research V52 turbine ~~is assumed to~~ have a S355 steel tower, with a measured tower geometry consisted of an 2.913 m outer diameter and 16 mm wall thickness.

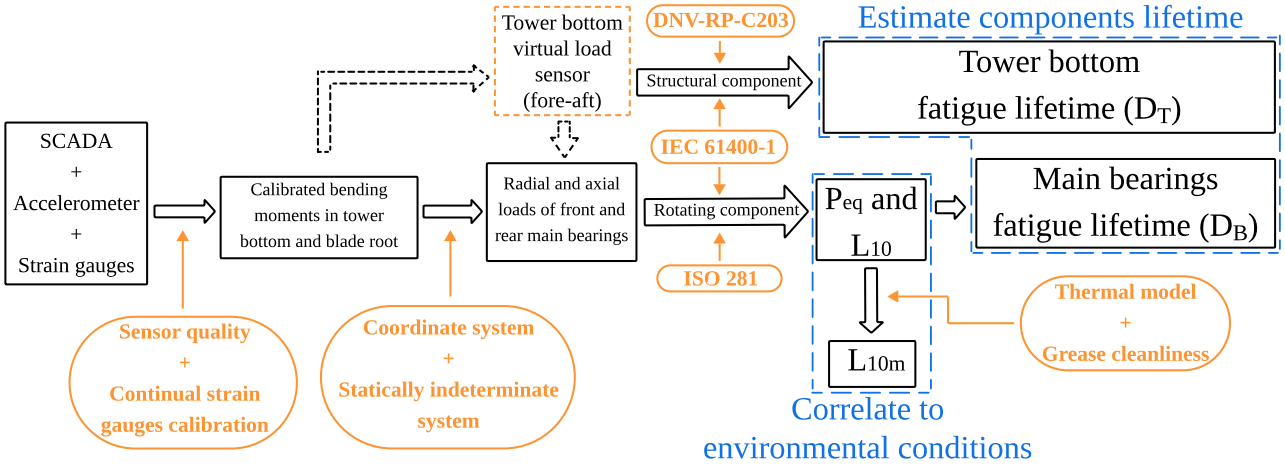

Figure 2. Methodology flowchart presenting the steps followed in this work, starting from high frequency measurement and SCADA dataset, to components lifetime estimates. Rectangular black boxes refers to measurement signals and estimates. Tower bottom D_T and main bearings D_B fatigue lifetime are analyzed over time, and the equivalent dynamic load P_{eq}, basic rating life L_{10} and modified rating life of the main bearing L_{10m} are analyzed as function of environmental conditions. Orange boxes identify the procedures and standards used in this work. The orange dashed box contains the tower bottom virtual load sensor, which should replace the real sensor in case of sensor failure.

In addition, a virtual load sensor is proposed to replace real strain gauges in the event of sensor failure and its performance is assessed for fatigue lifetime estimations. While, the main bearings equivalent dynamic load P_{eq}, the basic L_{10} and modified ~~$L_{10,m}$~~ L_{10m} rating life are evaluate as function of key environmental conditions. To compute the ~~$L_{10,m}$~~ L_{10m} of the main bearings, a drivetrain thermal model was made to estimate the temperature of the main bearings, which is necessary to estimate the life modification factor a_{ISO}, as introduced in Section 2.2.

4.1 Strain gauge zero-drift automatic calibration

It is often claimed that strain gauges are only reliable for short-term (less than a year) to mid-term (couple of years) campaigns, a limitation that would conflict with the requirement for sustained monitoring of wind turbine structural elements, most notably in offshore installations, where replacement in case of sensor failure is expensive and can take time due to weather windows.

This work overcomes such limitation by introducing continual and automated routines for the calibration of both tower bottom and blade root strain gauges that work on long-term datasets (almost a decade). The methods do not require operator intervention, stopping or curtailment, and instead take advantage of idling and parked conditions. Both methodologies are derived from the recommendations in IEC 61400-13 (2016). The main objective is to identify the artificial offset O from the measured strain gauges and to correct them to the original zero point. ~~No external dynamic load should cause zero strain.~~ The signals of the ~~bending moment~~ tower bottom and blade root bending moments shown in Figure 1 should be understood as $M = G \cdot (M_{raw} + O)$, where M is the corrected bending moment, M_{raw} is the measured ~~strain~~ voltage signal, G is the gain associated with the translation of voltage readings into bending moment, and O is the artificial offset of the strain sensor. It should be noted that for the tower bottom strain gauges placed on steel, G can be analytically calculated, depending on the bridge arrangement (full bridge Wheatstone in the DTU research V52 turbine), the elastic modulus and the geometry. However, for blade root strain gauges mounted on composite material, a blade pull exercise must be performed to estimate G. And a crosstalk correction has to be applied considering the geometry of the twisted and nonsymmetric blade, see Papadopoulos et al. (2000). Such calibration campaign has been undertaken on the DTU research V52 turbine, but the detailed results are not presented in this work for confidentiality reasons.

4.1.1 Yaw sweeps and Low-Speed Idling (LSI)

The tower bottom strain gauges calibration is based on a specific operation in which the wind turbine is parked and untwists its power cable at low wind speed. In that case, the turbine performs full yaw rotations and the main contribution to the tower bottom bending moment is the gravitational load from the nacelle mass ~~hanging~~ overhang bending moment. In case at least ~~1-minute~~ 1 min data points of the yaw angle γ are available, the high-frequency strain gauge signals M_xTB and M_yTB can be automatically calibrated Faria et al. (2024). The Python package generated for this matter is publicly available at Faria and Jafaripour (2023). The blade root strain gauge calibration is performed based on both idling and parked conditions at low wind speed. The first is used to calibrate the strain gauges placed on the pressure-suction surfaces of the blade. The latter is for those on the leading-trailing edges. The azimuth angle φ is needed at a higher sampling frequency (e.g. tested with at least 1 Hz). More information on the implementation can be found in Pacheco et al. (2024) and Faria et al. (2025).

4.2 ~~From blade and tower to main~~ Main bearing loads and temperatures

The front and rear main bearings of the DTU research V52 turbine are described in Table 1. The drivetrain transmits the torque from the rotor to the gearbox through the main shaft, which is supported by two spherical roller bearings in the main bearing housing and the gearbox upfront bearing as shown in Figure 3a.

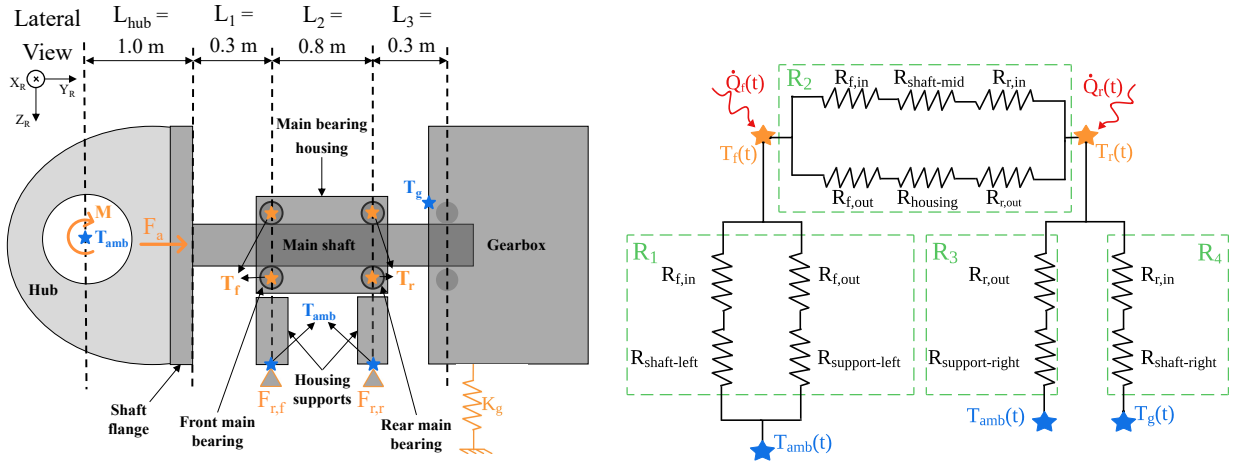

Figure 3. (a) Schematic of the DTU research V52 drivetrain and main bearings estimated front T_f and rear T_r temperatures. The hub carries the blades and their aerodynamic bending moment M and axial load F_a. The hub is bolted to the shaft flange. The shaft is supported by two main bearings, which are mounted inside the main bearing housing. The latter is clamped to the nacelle bedplate through the housing supports, ~~similarly~~ equivalent to the front $F_{r,f}$ and rear $F_{r,r}$ main bearings radial load F_r. The gearbox is mounted by the torque-arms but in ~~two~~ a non-rigidly stiff connection points with stiffness K_g. (~~b1~~b) ~~refers to~~ Simplified thermal circuit model of the ~~lateral view used to derive the vertical radial loads~~ drivetrain, which assumes that each 10 min instance reaches thermal equilibrium. Ambient temperature T_{amb} is measured in the ~~main bearing~~ nearby met-mast and ~~(b2) refers to~~ the ~~top view used to derive~~ gearbox temperature T_g is estimated based on a 6 months monitoring records of the ~~horizontal radial loads~~temperature of the gearbox wall facing the rear main bearing. ~~The M_v $\dot{Q}_r$~~ and ~~M_h $\dot{Q}_f$~~ are the ~~vertical and horizontal aerodynamic resultant bending moments from~~ dissipated power by the ~~rotor, while F_{rotor}~~ main bearings. R represents the equivalent thermal resistance: R_1 between front main bearing and ~~F_{shaft} are~~ ambient temperature; R_2 between main bearings; R_3 between rear main bearing and the ~~rotor~~ ambient and ~~shaft gravitational loads due to their weight~~ R_4 between rear main bearing and ~~M_{rotor} is~~ the ~~bending moment associated with the shift of F_{rotor} from the hub center~~ gearbox close surface to the ~~shaft flange by L_{hub}~~rear main bearing. ~~As for the reactions, radial loads~~ Other heat exchanges are ~~given by R, classified as $_r$ for rear, $_f$ for front, $_v$ for vertical and $_h$ for horizontal~~not considered. The ~~gearbox mounting stiffness is equally estimated in both direction~~ $R_{(\_,\_)}$ are estimates on geometry of the drivetrain components (assumed as steel) and ~~represented~~ bearings heat transfer coefficients suggested by ~~the spring K_g~~Schaeffler TPI-176 (2014).

The main bearing housing is clamped to the nacelle bed plate, while the gearbox is mounted through its torque-arms in a rubber support. The rubber support is assumed to have a linear and temperature-independent spring with a stiffness of $20{\cdot}10^6$ [N/m], close to the ~~suggested values~~ values suggested in Haastrup et al. (2011); Keller et al. (2016). ~~A~~ In Section 5.5.1, a sensitivity analysis is performed ~~later~~ to evaluate the importance of this assumption. ~~The static gravitational loads acting on the main shaft, shown in Figure **??**, are derived from a combination of public sources and visual inspections of the turbine nacelle. Similar for the lengths (e.g. L_{shaft}). The gravitational force of the rotor F_{rotor} is calculated assuming a rotor and a hub mass of 10 tons (third party source, see Scribd (2021)). The gravitational force of the shaft F_{shaft} assumes a shaft mass equal to 1~~

~~ton, between an internal estimate of 0.8 tons and the Fingersh et al. (2006) estimate of 1.2 tons, which uses the best-fit equation~~

~~$m_{shaft} = 0.0142 \cdot D^{2.888}$ from historical data (given D as the rotor diameter in meters and the mass in tons).~~

Table 1. Technical specification of the two main bearings in the DTU research V52 turbine given by SKF Group (2025). SRB stands for spherical roller bearing and the bearing ~~p is equal to $10/3$~~exponent $p = 10/3$.

Main bearing	Designation	Type	Inner diameter	Outer diameter	Basic dynamic load rating C_d	Basic static load rating C_o	Fatigue load limit C_u	limiting factor e
Front	23064	SRB	320 [mm]	480 [mm]	2348 [kN]	3800 [kN]	285 [kN]	0.23
Rear	23160	SRB	300 [mm]	500 [mm]	3368 [kN]	5100 [kN]	380 [kN]	0.3

~~Once static loads are defined, the~~ The aerodynamic bending moment M driven by the blades in the vertical M_v and horizontal M_h directions can be estimated from the blade out-of-plane bending moments, using:

$$M_v(t) = M_{flapwise,A}(t) \cdot \cos(\varphi(t)) + M_{flapwise,C}(t) \cdot \cos(\varphi(t) + 120) + M_{flapwise,B}(t) \cdot \cos(\varphi(t) + 240) \quad (12)$$

$$M_h(t) = M_{flapwise,A}(t) \cdot \sin(\varphi(t)) + M_{flapwise,C}(t) \cdot \sin(\varphi(t) + 120) + M_{flapwise,B}(t) \cdot \sin(\varphi(t) + 240) \quad (13)$$

where $\varphi(t)$ is the azimuth angle of blade A, see Figure 1. It should be noted that a positive M_v should benefit the loads in the radial main bearings to some extent, as it counter-balances F_{rotor}.

The main shaft is supported in ~~3~~ 4 points, two main bearings and the gearbox ~~, in both directions (lateral view and top view), so it is~~ mounts, and it is solved as a statically indeterminate system. ~~To solve it~~The radial clearance from the bearings is not explicitly considered. To solve the system of equations, the shaft is modeled as a flexible beam and a double integration method is applied to compute the radial load ~~$R_{f,v}$, $R_{f,h}$, $R_{r,v}$ and $R_{r,h}$~~ of the front $F_{r,f}$ and rear $F_{r,x}$ main bearings (see Appendix B). Both aerodynamic and gravitational loads are included to estimate the radial loads. The resultant radial loads of the front ~~R_f and rear R_r~~ $F_{r,f}$ and rear $F_{r,x}$ main bearings have a magnitude of

$$R_{(f,r)}F_{r,(f,r)} = \sqrt{R^2_{(f,r),v} + R^2_{(f,r),h}}\sqrt{F^2_{r,(f,r),v} + F^2_{r,(f,r),h}} \quad (14)$$

~~, which~~ where v represents the vertical direction and h the horizontal direction (no static gravitational loads) as shown in Appendix B, and are solved individually for each main bearing.

The axial load F_a of the main bearings is equal to the thrust estimate, derived as the bending moment $M_{fore-aft}$ divided by the height difference between the hub height and the tower bottom strain gauge. This is an assumption of this methodology, where the thrust estimate is linearly related to the bending moment of the bottom of the tower. ~~Apart from that, since both bearings are able to carry axial load~~Since both bearings can carry axial loads, the system ~~could~~ may become over-constrained~~.~~ ~~An additional axial load would be applied to the bearings in the case of~~ , causing additional axial stress during thermal expansion. For these reasons, the rear bearing is considered the locating bearing, being the larger bearing ~~between the two.~~ and with greater axial internal clearance.

Drivetrain thermal model

In case the temperature measurements of the main bearings are not available, estimates of the temperature of the main bearings are necessary to incorporate the life modification factor a_{ISO}. The a_{ISO} is a function of viscosity, which is a function of the lubricant temperature. Figure 3a shows the estimated temperatures from the rear T_r and front bearing T_f, together with the measured temperatures, ambient T_{amb} and gearbox wall T_g. It is proposed to simplify the heat exchange between the heat dissipated by the bearings and the outer system (drivetrain), assuming thermal equilibrium in each 10 min instance and thermal resistors, as shown in Figure 3b. The ambient temperature T_{amb} is measured using a spinner anemometer at the hub and the gearbox temperature T_g is estimated based on 6 month monitoring campaigns that recorded the temperature of the gearbox wall facing the rear main bearing. A SCADA-based Feedforward Neural Network (FNN) model was trained to estimate the values of T_g for each 10 min instance.

$$\dot{Q}_f - \frac{(T_f - T_{amb})}{R_1} - \frac{(T_f - T_r)}{R_2} = 0 \tag{15}$$

$$\dot{Q}_r + \frac{(T_f - T_r)}{R_2} - \frac{(T_r - T_{amb})}{R_3} + \frac{(T_g - T_r)}{R_4} = 0 \tag{16}$$

By applying the Kirchhoff circuit concept for thermal equilibrium, Equations 15 and 16 are obtained, which have two target variables T_f and T_r, and the thermal resistances R_i defined in Figure 3b. The dissipated power of a bearing is also affected by the bearing temperature (e.g., $\dot{Q}_f = f(T_f, ...)$), as the latter influences the viscosity of the lubricant (the base oil of the grease according to ASTM D341-93 (1998)). Because the variables depend on one another, the equations are coupled and cannot be solved explicitly. Instead, a Newton-Raphson solver was implemented to iteratively estimate the results. This framework can be found in more detail in HIPERWIND D5.1 (2023). The dissipated powers were modeled as suggested by Schaeffler TPI-176 (2014), which separates them into two contributions: frictional heat driven by speed and frictional heat driven by load. The grease has been assumed as Klüberplex BEM 41-301, a widely distributed industrial grease for wind turbine main bearings. Once T_r and T_f are estimated, the a_{ISO} can be calculated as a function of viscosity ratio κ, assumed grease cleanliness level (see Section 5.5.3), C_u and P_{eg} as given by ISO-281 (2007).

4.3 Tower bottom virtual load sensor: thrust and fatigue loads

The selection of good candidates for the machine learning model to be deployed as virtual load sensors was carried out from simpler to more complex neural network architectures. Pure spatial correlation between the target variable and inputs is tested using a ~~feedforward neural network (FNN)~~ FNN baseline model (Rumelhart et al., 1986). Temporal correlation is added through an FNN with n-lagged time steps, ~~NlaggedFNN Dimitrov and Göçmen (2022)~~the so called NlaggedFNN (Dimitrov and Göçmen, 2022), and a Long Short-Term Memory (LSTM) neural network (Bengio et al., 1994). The first can only take a few time steps to still be "trainable", while LSTM is often a less noise sensitive model and can better capture long-term dependencies ~~according to Bengio et al. (1994)~~(Bengio et al., 1994), at the cost of model complexity. The hyperparameters of the models were tuned using the Keras-tuner random search method O'Malley et al. (2019) using ~~5~~ 10 h

of data and 3 seeds per iteration. The bounds and the optimal hyperparameters for the models ~~that combine all possible inputs~~ are included in Appendix C. All models used the "relu" activation curve in the hidden layers and "linear" activation towards the output layer. The LSTM model had a fixed "LSTM" layer and a second hidden layer with the same amount of neurons (hidden units) as the first layer. The size of the training data set was 160 h of data selected using a ~~k-means~~ K-means clustering technique Pedregosa et al. (2011), spreading the training space within the rotor speed, blade pitch, power, and ~~design load cases (DLC)~~ DLCs to cover the relevant operational conditions. Similarly to Dimitrov and Göçmen (2022), a training dataset size and sampling frequency sensitivity were carried out to use optimum values. In addition to that, different input signals are tested. Starting from most available "SCADA" alone, including blade pitch, rotor speed, power, and azimuth (which was converted into sine and cosine), then either adding ~~tower top~~ nacelle "Accelerometer", or the ~~flapwise bending moment~~ M_xBR blade root bending moments from one or all blades (stated as "Strain"). And finally combining all available inputs as "All".

Figure 4 shows the power spectrum density (PSD) of the different normalized input signals. One hundred representative instances around the rated wind speed and similar turbulence and shear were analyzed. ~~The different dynamic components with which the neural networks will be trained is visualized. It can be seen that all SCADA signals a high quasi-static component, while the azimuth has pronounced spikes around 1P, 3P, and 6P.~~

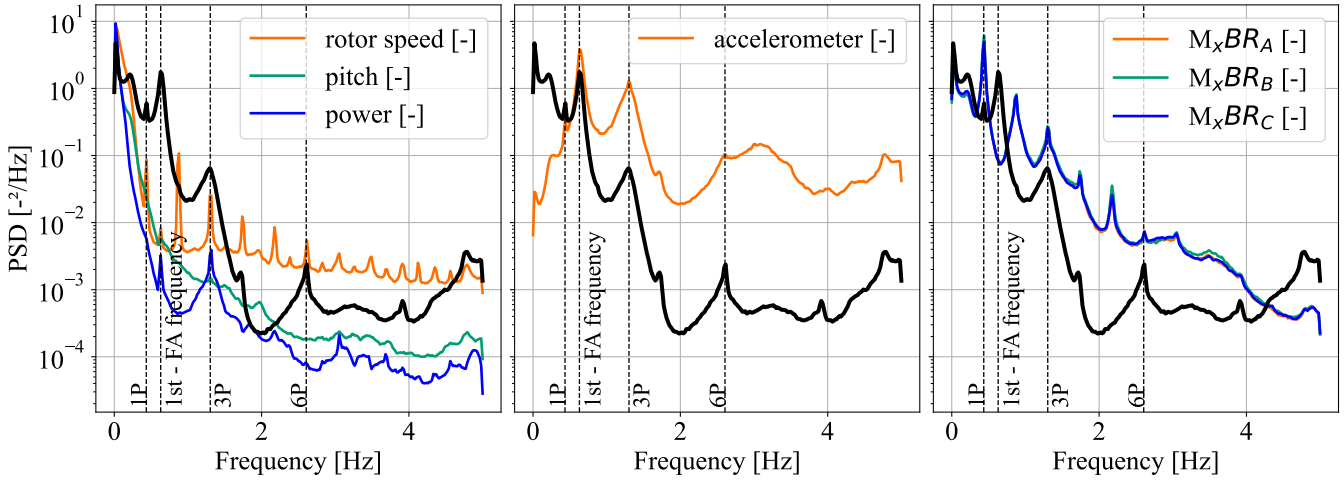

Figure 4. Normalized Power Spectrum Density (PSD) of the possible input signals to be used in the training of a time-series virtual load sensor: SCADA (left), nacelle accelerometer (middle) and blade root bending moments (right). The black line is added in all charts as is the target variable $M_{fore-aft}$ of the virtual load sensors. Normalization is based on the 10 min instance mean and standard deviation of ~~each 10-min instance and~~ signal. The spectrum is generated by averaging 100 instances at rated wind speed (14 m/s)~~to generate a smooth PSD chart~~. Dashed vertical lines indicate the rotor frequency (1P), the blade passing frequency (3P) and the higher harmonics as well as the first fore-aft (FA) tower resonance.

However, only the accelerometer ~~signal can well capture~~ input signal can capture well the first fore-aft turbine frequency (around 0.62 Hz Rinker et al. (2018)), present in the target variable $M_{fore-aft}$, while its amplification of higher frequency components compared to $M_{fore-aft}$ ~~cannot be~~ is not considered pure electrical noise. When testing in standstill/parked

conditions, there is a strong attenuation similar to the $M_{fore-aft}$ PSD. The most consistent explanation is that the gearbox operation feeds high-frequency broadband vibrations ~~through the bedplate into the nacelle accelerometer, elevating the spectrum beyond a discrete peak.~~

to the nacelle accelerometer mounted below the bedplate near the gearbox. Virtual load sensors trained on the nacelle accelerometer might add higher frequency oscillations to the $M_{fore-aft}$ estimate, as shown in Figure 8. The performance metrics selected are the Normalized Root Mean Square Error (NRMSE), which is normalized by the standard deviation σ_y instead of the mean signal to avoid overshoot in case of small mean values. To validate fatigue lifetime estimates, the equivalent damage load DEL and P_{eq} are analyzed in terms of the mean absolute error (MAE).

$$\text{NRMSE} = \frac{1}{\sigma_y}\sqrt{\frac{\sum_{i=1}^{N}(Y_{\text{pred},i} - Y_{\text{meas},i})^2}{N}} \tag{17}$$

$$\text{MAE}_{Load=(DEL,P_{eq})} = \frac{1}{N}\sum_{i=1}^{N}\left|\frac{\text{Load}_{\text{pred},i} - \text{Load}_{\text{meas},i}}{\text{Load}_{\text{meas},i}}\right| \times 100 \tag{18}$$

where Y_{pred} is the time instant prediction, Y_{meas} is the measured of $M_{fore-aft}$, and N is the number of instances ~~included.~~ evaluated.

4.4 ~~Drivetrain thermal model~~

~~(a) Schematic of DTU research V52 turbine drivetrain with the main bearing estimated front and rear temperature T_f and T_r. Ambient temperature T_{amb} is measured in the nearby met-mast and the gearbox temperature T_g is estimated based on a 6 months monitoring campaigns which recorded the temperature of the gearbox wall facing the rear main bearing. (b) Simplified thermal circuit model of the drivetrain, which assumes that each 10-min instance reaches thermal equilibrium and average values of load, temperature and heat are estimated. $\dot{Q}_r$ and $\dot{Q}_f$ are the dissipated power by the main bearings. R represents the equivalent thermal resistance: R_1 between front main bearing and ambient temperature; R_2 between main bearings; R_3 between rear main bearing and the ambient and R_4 between rear main bearing and the gearbox closest surface to the main bearing housing. Other heat exchanges are not considered. The $R_{(...)}$ are estimates on geometry of the drivetrain components (all assumed as steel) and bearings heat transfer coefficients suggested by Schaeffler TPI-176 (2014). To incorporate the life modification factor a_{ISO} in the evaluation of the main bearings, estimates of the main bearings temperature are necessary, as the first is function of viscosity which is function of temperature. Figure **??** shows the estimated temperatures from the rear T_r and front bearing T_f, together with the measured temperatures, ambient T_{amb} and gearbox wall T_g. It is proposed to simplify the heat exchange between the heat dissipated by the bearings and the outer system (drivetrain), by assuming thermal equilibrium in each 10 min instance and thermal resistors, as shown in Figure 3b. The ambient temperature T_{amb} is measured by a spinner anemometer at the hub and the gearbox temperature T_g is estimated based on 6 month monitoring campaigns that recorded the temperature of the gearbox wall facing the rear main bearing. A SCADA-based small FNN model was trained to estimate values of T_g for each 10-minute instance, and it yielded 3 °C MAE, which is reasonable considering the scope of this investigation.~~

$$\dot{Q}_f - \frac{(T_f - T_{amb})}{R_1} - \frac{(T_f - T_r)}{R_2} = 0$$

$$\dot{Q}_r + \frac{(T_f - T_r)}{R_2} - \frac{(T_r - T_{amb})}{R_3} + \frac{(T_g - T_r)}{R_4} = 0$$

By applying the Kirchhoff circuit concept for thermal equilibrium, Equations **??** are obtained, which have two target variables, T_f and T_r. However, the dissipated power of a bearing is also affected by the bearing temperature (e.g., $\dot{Q}_f = f(T_f, ...)$), as the latter influences the viscosity of the lubricant (the base oil of the grease). Because the variables depend on one another, the equations are coupled and cannot be solved explicitly. Instead, a Newton-Raphson solver was implemented in Python to iteratively estimate the results, and no convergence issue was encountered. This framework can be found in more detail in HIPERWIND D5.1 (2023). The dissipated powers were modeled as suggested by Schaeffler TPI-176 (2014), which separates them into two contributions: frictional heat driven by speed (and viscosity ν) and frictional heat driven by load. The grease has been assumed as Klüberplex BEM 41-301, a widely distributed industrial grease for wind turbine main bearings. Once T_r and T_f are estimated, the viscosity of the base oil is calculated according to ASTM D341-93 (1998). Lastly, a_{ISO} can be calculated as a function of viscosity ratio κ, grease cleanliness level, C_u and P_{eq} as given by ISO-281 (2007).

5 Results

5.1 Continual calibration routines

Figure 5 shows the identified calibration factors for each of the two tower bottom strain gauges and the six blade root strain gauges, all converted to bending moments as explained previously in Section 4.1. The charts to the right in both Figures 5a and 5b show the "Sensor position" represent the angle difference of the installed sensor with respect to the SCADA reference variable, the yaw angle γ for the tower (cardinal north as the zero point) and the azimuth angle φ for the blade sensors (blade A upward as the zero point). Automatic routines manage to identify the position of the sensors correctly with a standard deviation (std) of less than 4 degrees, even though the azimuth correction explained in the Appendix A was not applied at this stage, leading to higher variability before 2018 and after 2022.

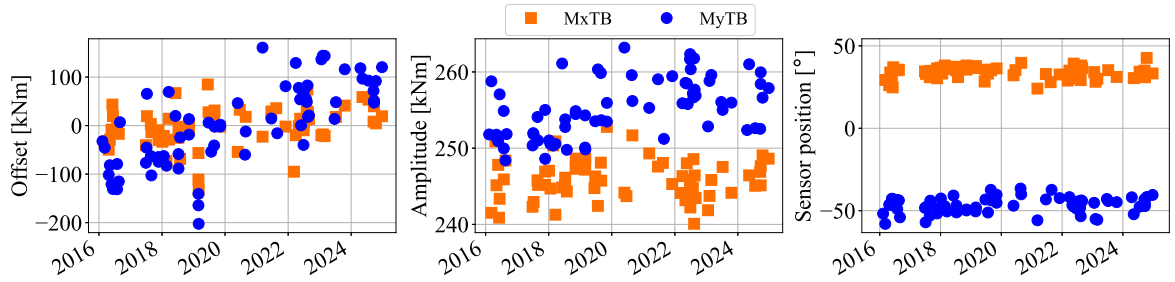

(a) Tower bottom strain gauge bridges

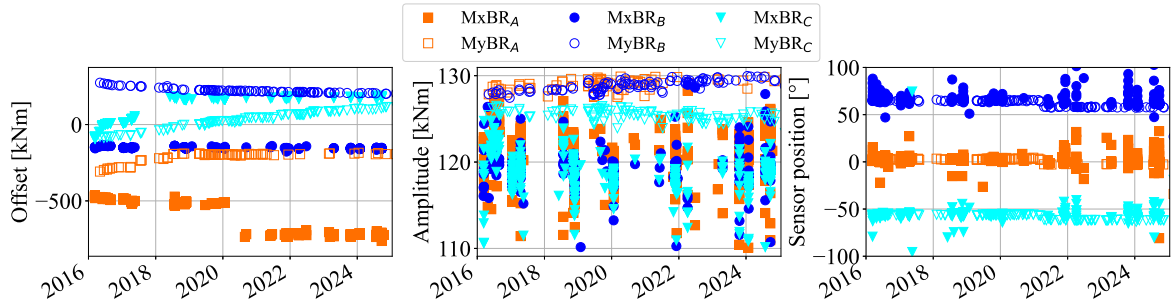

(b) Blade root strain gauge bridges

Figure 5. Identified calibration factors from 2016 to 2024 (inclusive), including offset (left), amplitude (middle), and sensor position (right) of strain gauges installed in the (a) tower bottom using yaw sweep routines and (b) blade root using Low-Speed Idling (LSI) routines. The position of the tower bottom strain gauges bridge is defined with respect to the yaw angle $\gamma(t)$. The position of the blade root strain gauges bridge is defined with respect to the azimuth angle $\varphi(t)$. (a) Note that the mean offset value has been subtracted from each strain gauge bridge in the tower bottom for clarity, with a mean of 1240 kNm and -3326 kNm for M_xTB and M_yTB, respectively.

From the left charts, it is possible to observe larger zero drifts for the blade root compared to the tower bottom strain gauges. The M_xBR_A, M_yBR_A, and M_xBR_C also present an abrupt change in the zero drift in 2018 and 2020. This could be justified by sensor replacement or data acquisition settings; however, no final explanation has been validated. ~~. The amplitude~~ The amplitude (middle charts) in this method is the maximum gravitational overhang bending moment. In the case of the yaw sweep, driven by the rotor-nacelle weight in respect to the tower bottom (Faria et al., 2024), and for the LSI, driven by the blade weight in respect to the blade root (Faria et al., 2025). To have a quantitative accuracy quantification of the automatic routines in identifying the offset and the amplitude their unexplained variability are normalized by reference values: the mean $M_{fore-aft}$ bending equal to 3540 kNm for the tower strain gauge and the mean $M_{flapwise_{(A,B,C)}}$ bending equal to 500 kNm for the blade strain gauges, both at rated wind speed. From the middle chart in Figure 5a, an amplitude ~~std~~ standard deviation of less than 4 kNm (equal to 0.04 MPa) can be observed for both sensors, which represents a variability of 0.1% to the tower reference. For the blade, an amplitude std less than 3 kNm, representing a 0.6% variability.

~~Identified calibration factors for a period of nearly 9 years, including offset, amplitude and sensor position. Each marker represents one identified yaw sweep for the tower bottom strain gauges and its calibration factors(a) and one Low-Speed Idling (LSI) for the blade root strain gauges and its calibration factors (b). In average, 2 calibration instances are available per month. The tower bottom sensors position is defined in respect to the yaw angle $\gamma(t)$. The blade root sensor position is defined in respect to the azimuth angle $\varphi(t)$.~~

The larger variability from the blade root strain gauges calibration factors could be explained by the fact that its Wheatstone bridge is compensated for temperature differences in the whole blade, but not for temperature gradients between the two blade surfaces. Once the offsets, shown in the left charts, are used to remove the artificial zero drift from the sensors, there will still be residuals that are not explained by the automatic routine. The offset residuals of the tower showed a std of less than 60 kNm (corresponding to 0.5 MPa), which is 1.6% of the reference. While, for blade strain gauges, the offset residuals had an std of less than 10 kNm, representing a variability of 2%.

5.2 ~~Lifetime~~ Fatigue lifetime of tower and main bearings

5.2.1 ~~Fatigue damage accumulation~~

Once all strain gauges have been calibrated and high-frequency measurements and SCADA are available, the long-term lifetime can be estimated over time, as shown in Figure 6. Considering that failure is reached at unity, the basic lifetime of the main bearing L_{10} can be evaluated using Equation 7.

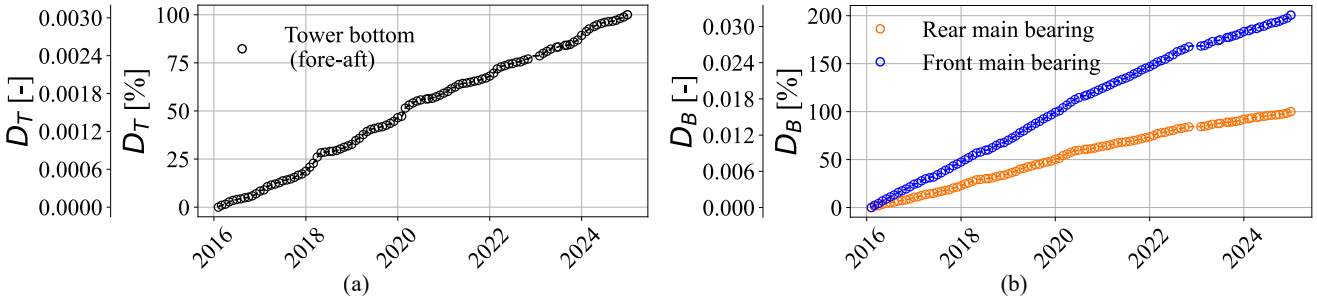

Figure 6. Fatigue damage accumulation of (a) the tower (structural component) and (b) the main bearings (rotating components) of the DTU research V52 turbine from 2016 to 2024 (inclusive). Fatigue damage was counted according to Equations 2 and 7. Charts have an absolute accumulation and a normalize y-axis in respect to the end measured accumulated damage (D_B is normalized based on the rear main bearing).

The front bearing $L_{10,f}$ is ~~166~~ 282 years and the rear bearing $L_{10,r}$ is ~~333~~ 566 years. Similarly, the tower has a even larger lifetime of ~~1770~~ 2952 years. This significantly longer lifetime, compared to the design lifetime of 20 years proposed by IEC 61400-1 (2019), is in part justified by the low wind potential of the Risø site, as discussed in Section 3. However, it also points to the fact that older and smaller turbines, such as the DTU research V52 turbine, have long remaining useful lifetimes (RUL) of key components that should be considered in lifetime extension (LTE) decisions. ~~Fatigue damage accumulation of (a) the tower (structural component) and (b) the main bearings (rotating components) of the DTU research V52 turbine for 9 years.~~

~~Fatigue damage was counted according to Equations 2 and 7. Charts have an absolute accumulation and a normalize y-axis in respect to the end measured accumulated damage (normalization of D_B considers the rear main bearing).~~

5.2.1 Linear zero-drift assumption and simple uncertainty propagation to tower and main bearing lifetime.

It is proposed to assume linear zero drift of the different strain gauges offsets as a single linear function or a combination of linear functions, which can be derived from continuous calibration factors over time. Then it is important to quantify the uncertainty of this assumption in the life of the main bearings, which is based on the absolute load values P. ~~Figure ?? shows how this~~ The analysis was carried out ~~to evaluate the effect on main bearing basic rating life L_{10} as described by Equation 6. Representative 10-min~~ by fitting the linear functions to the offsets and storing the residuals of the fit. Representative 10 min instances (DLCs 1.2, 3.1 and 4.1) were used to estimate the main bearing rating lifetime $L_{10,j}$ assuming ~~a~~ an offset with Gaussian distribution derived from the residuals from the fitting function. Then 10000 Monte Carlo iterations were carried out calculating the $L_{10,j}$ based on a random selection of the offset Gaussian distribution. For all three instances, the ~~std~~ standard deviation of both bearings $L_{10,j}$ was below 0.7%. Similar analysis was carried out for the fore-aft fatigue load ~~. However, fatigue~~ DEL and even negligible standard deviation was found. Fatigue is not affected by the mean load value (as described in Equation 2) and is then not sensitive to the offset, assuming there are no large yaw angle variations within 10 min instances, see Equation 9. ~~Uncertainty quantification flowchart to estimate the variability in the main bearings basic lifetime $L_{10,j}$ in a 10 min instance j due to the linear assumption of the zero-drift strain gauges once continual calibration is applied. Each strain gauge offset is randomly sampled from its deterministic linear fit and the residuals distribution. Monte Carlo is applied for 10000 iterations.~~

5.2.2 ~~Effect of periodic calibration on the main bearings L_{10}~~

Effect of periodic calibration on the main bearings L_{10}

Now that continuous calibration with linear zero drift has been defined as the benchmark with a error less than 1%, it is sought to understand how periodic calibration of strain gauges, as often carried out in the industry, ~~could affect~~ can influence the lifetime estimation of ~~the main bearings~~ main bearings for this methodology. Table 2 shows the difference between the L_{10} measured ~~over 9 years~~ from 2016 to 2024 (inclusive) with continual calibration compared to ~~the periodic calibrationscarried out~~periodic calibrations. The absolute results of L_{10} error due to calibration periodicity are not generalizable, as they are influenced by the zero drift behavior of each monitoring setup and the ~~absolute~~ loads of the wind turbine. However, it highlights ~~how severely~~ poor strain gauge calibration ~~can influence~~ influences the lifetime estimation of main bearings for this methodology.

Table 2. Error in the L_{10} estimation for ~~7.5 years~~ from 2016 to 2024 (inclusive) as a function of how often strain gauges are calibrated.

	Monthly	3-months	6-months	Yearly	2-year	4-years	At commissioning
L_{10} error [%]	8.0	9.3	11.9	13.1	34.8	70.5	90.6

5.3 Virtual load sensor performance validation

~~More than~~ A 160 h of training ~~data were~~ dataset was used, as no significant improvements were found by enlarging the dataset, while downsampling from 50 Hz to 10 Hz remained within the error convergence. The latter could decrease the dynamic content and underestimate the measured fatigue damage; therefore, to verify this, a procedure proposed by D'Antuono et al. (2023) was carried out, and sampling frequencies lower than 8 Hz contained more than 98% of the measured fatigue damage in representative instances, to all considered ~~design load cases (DLCs)~~DLCs. A sampling frequency of 10 Hz is used.

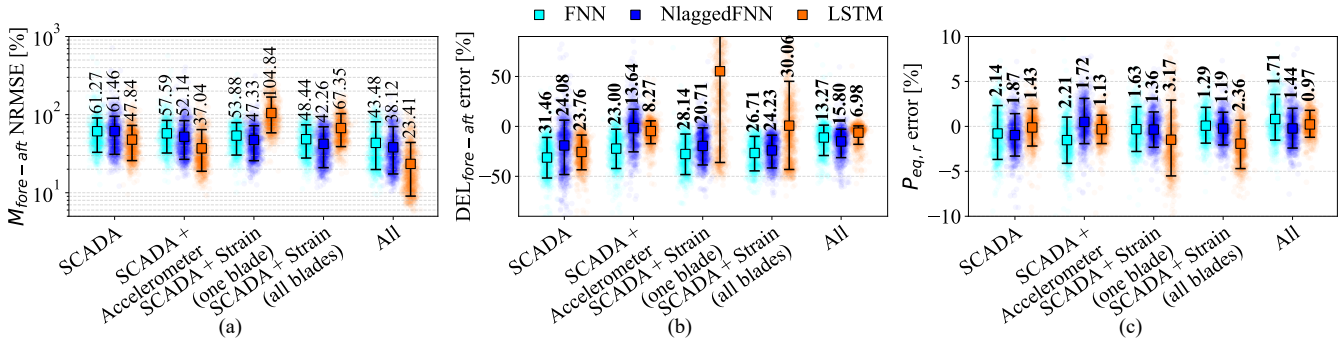

Figure 7. Virtual load sensor validation performance applied to 160 hours of measurements. Their performance is shown based on the 3 metrics described in Equations 17 and 18. The different columns represent the feature selected as inputs and the different colors the model type (neural network architecture). The box-plots show the mean value and the 10^{th} and the 90^{th}. The number in the left subplot are the mean value of the NRMSE, whereas the bold values in the middle and right subplots, have the mean absolute error (MAE).

The 15 different combinations of virtual load sensors (5 input options and 3 model types) are validated using 160 h ~~from the 2019.~~ of data from the 2019, also selected using K-means clustering technique. From left to right, Figure 7 presents all combinations of models tested in terms of the metrics shown in Equations 17 and 18: including NRMSE $M_{fore-aft}$ (a), MAE $DEL_{fore-aft}$ (b), and MAE P_{eq} (c). Raw data are added for completeness as transparent markers. ~~It can be seen that the~~ The LSTM model with "All" inputs outperforms the other models significantly when comparing NRSME. The mean error of ~~23.41~~23% is almost half the second-best performing model combination (LSTM and "SCADA + Accelerometer"), which yields 37%. However, when no accelerometer signal was included and blade strain gauges were added, the LSTM performance worsened compared to the FNN and NlaggedFNN models. ~~It seems that LSTM cannot attenuate the pronounced~~ The LSTM added unrealistic oscillations in the time-series estimate with larger 1P, 2P, and 3P ~~contributions of the blades, without a clear estimate of the first fore-aft frequency component (present in the accelerometer signal)~~frequency contributions and underpredicted the 1^{st} FA frequency contribution, most likely due to poor model coupling of the blade strain gauges and azimuth angle φ inputs. The NlaggedFNN was chosen when no accelerometer was available in the input. Regarding the equivalent load of the main rear bearing $P_{eq,r}$, influenced by the thrust estimate from the virtual load sensors, ~~it is observed a overall negligible difference~~ a negligible difference is observed between all combinations of models. Models ~~using only "SCADA " already reach MAE errors below~~ with only SCADA reached MAE errors of 2%. ~~The same results were found for~~

~~long-term deployment over 7.5 years~~For the deployment from June 2017 to 2024, all models ~~within 2% of~~ had an error below 10% compared to the measured main bearing L_{10}~~estimates~~ lifetime.

For the equivalent damage loads at the tower bottom fore-aft $DEL_{fore-aft}$, models solely using SCADA had a minimum MAE error of 23.76%. Looking at Figure 8, it can be observed that the model with SCADA (LSTM) had an overprediction for very low amplitude cycles, while underprediction for larger amplitude cycles. This becomes more predominant for above rated wind speed conditions (refer to Figure 8b). Looking at its PSD, the model also does not properly capture the frequency components of the reference signal $M_{fore-aft}$. Adding the accelerometer yielded strong improvements. The best performing combination with "SCADA + Accelerometer" and LSTM had an MAE of 8.27%, very close to the overall best performing combination of "All" and LSTM with 6.98%.

~~Stress cycle histogram and Power Spectrum Density (PSD) chart (inset top right) of tower bottom $M_{fore-atf}$ estimate for the different input signal combined with their best performing model compared to the measured (black). All stress histograms are the summation and the PSD charts the averaging of 100 instances from 2019. (a) Below rated wind speed 8 m/s (DLC 1.2). (b) Above rated wind speed 16 m/s (DLC 1.2). (c) Start-up and shutdown (DLC 3.1 and 4.1)~~

~~The~~ And the models that included strain without accelerometer have ~~a worsened performance of 20.71% and 24.23% for the best combination with NlaggedFNN, and also~~ included undesired, sharp and narrow-band peaks, most likely coming from the blade modes, that are not transmitted to the tower in reality~~.~~, see Figure 8 "SCADA + Strain (one blade) or (all blades).

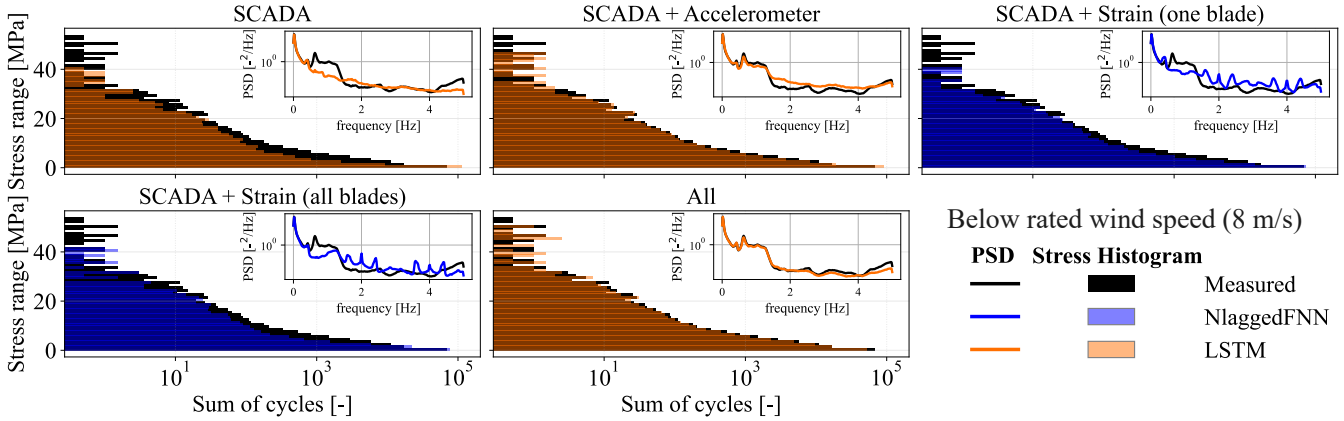

(a)

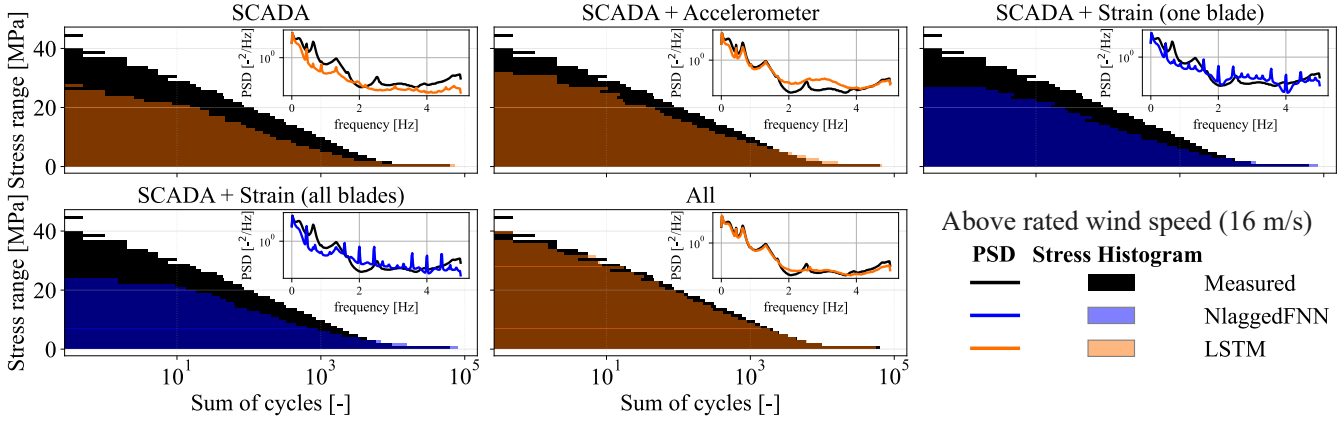

(b)

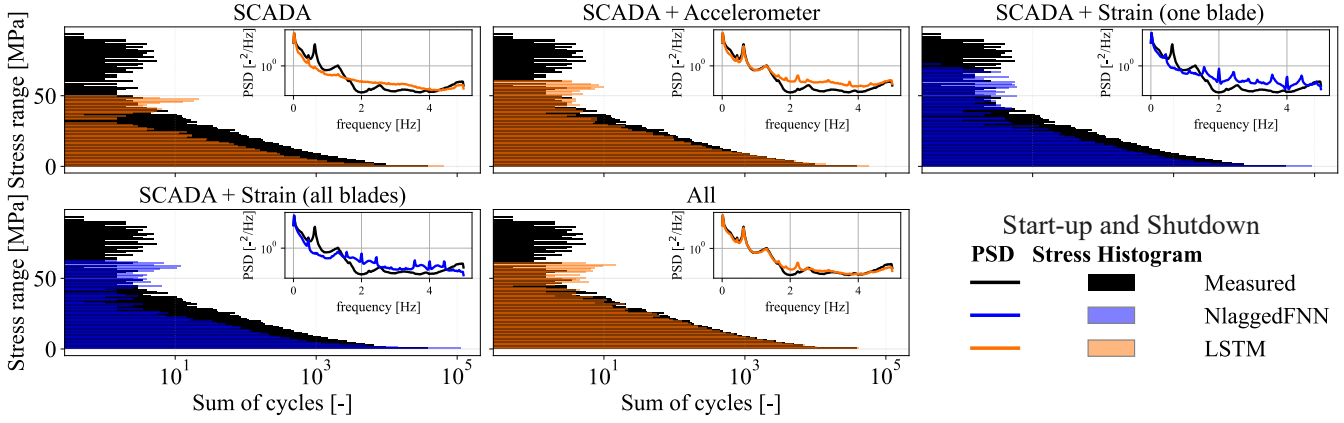

(c)

Figure 8. Stress cycle histogram and Power Spectrum Density (PSD) chart (inset top right) of tower bottom $M_{fore-aft}$ estimate for the different input signal combined with their best performing model compared to the measured (black). All stress histograms are the summation and the PSD charts the averaging of 100 instances from 2019. (a) Below rated wind speed 8 m/s (DLC 1.2). (b) Above rated wind speed 16 m/s (DLC 1.2). (c) Start-up and shutdown (DLC 3.1 and 4.1)

Looking close to the two best performing model combinations overall, "SCADA + Accelerometer" and "All" with LSTM, it is worth taking a closer look at Figures 8a and 8b. It is observed that only the model "All" is consistent in predicting stress ranges at both below and above rated wind speed, while rarely overpredicting the energy content for frequencies components above 0.62 Hz. ~~Figure 8c shows the models performance under~~ However, as shown in Figure 8c for DLC 3.1 and 4.1~~together. Again, LSTM with "All" shows the most consistent results. However,~~ , all the possible combinations under-predict large ~~oscillations, and consequently large stress ranges~~stress ranges, probably due to the lack of downwind oscillations from the blade root strain gauges once the blade is fully pitched.

5.4 Tower fatigue estimation using virtual load sensors

LSTM is chosen as the best model to combine with "SCADA", "SCADA + Accelerometer", and "All", while NlaggedFNN is chosen for "SCADA + Strain" (one and all blades). The long-term deployment of these is ~~then~~ performed to verify their reliability in estimating the ~~lifetime of the tower . Unfortunately, since~~ tower fatigue. Since the high-frequency database before ~~July~~ June 2017 is sampled at 35 Hz, in contrast to 50 Hz after ~~July~~ June 2017, the results related to the implementation of virtual load sensors do not include ~~this initial period, as the models were trained on 10 Hz data~~the 35 Hz dataset. Downsampling 35 Hz to 10 Hz requires interpolation~~rather than a clean decimation (50 Hz to 10 Hz)~~, which may affect consistency. Figure 9 shows the accumulated tower fatigue damage of each virtual load sensor combination D_T normalized by the final accumulated damage~~measured~~. It is interesting to note that more damaging contributions are present at the beginning of each year because the Danish winter has higher wind speeds. ~~In terms of virtual load sensors, all~~ All combinations of models have underpredicted the accumulated damage (under-conservative), which is expected by looking at the analysis ~~done~~ performed during validation and shown in Figure 8. The difference between the best-performing model "All" and the second model "SCADA + Accelerometer" is equal to 11%, from 64% to 75%. The remaining three models perform considerably worse in the long term with estimates below 30% of the reference damage.

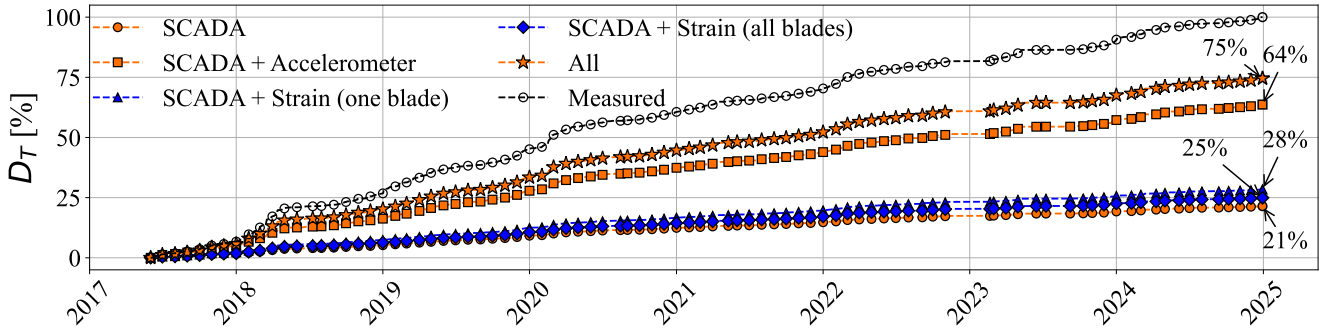

Figure 9. Tower bottom fore-aft fatigue damage accumulation comparison between different virtual load sensors models. It shows the total accumulation ~~for a period of 7.5 years~~ from June 2017 to 2024 (inclusive) normalized, for the sake of comparison, by the final measured fatigue accumulated damage. The different model combinations are shown by inputs used (marker) and by model type (marker fill color). The latter for sake of consistence maintains the colors from Figure 7, blue for NlaggedFNN and orange for LSTM.

5.4.1 Proposed experimental slope correction for tower damage accumulation and statistical uncertainty

If a virtual load sensor is consistent throughout the majority of operating conditions over the year, it would underestimate different years with a similar error. Figure 10a shows the comparison for a full year (2018 as the first round year available) of estimated and measured accumulated damage. The slope η_k represents the under-prediction ratio, calculated as the linear fit slope between the estimate and the measured accumulated damage yearly. ~~And the greater the linear fit coefficient of determination R^2 , the lower the unexplained variability of the linear fit of a given virtual load sensor.~~ Then, one could have an accumulated damage from the virtual load sensor adjusted by the yearly slope as in

$$D_{T,a} = \frac{D_{T,vls}}{\eta_k} \tag{19}$$

where $D_{T,vls}$ is the original and $D_{T,a}$ is the adjusted accumulated damage of the virtual load sensor. The slope η_k is the linear fit slope between the virtual load sensor and the measured damage for a given year k, and it is used as a correction factor.

~~An issue with the~~ The proposed experimental correction is the error associated with the choice of a given year k to calculate the slope by chance. Figure 10b shows the calculated η_k for each year~~independently.~~ . Note that small differences in annual mean wind speed were measured (see Section 3). The "All" and "SCADA + Accelerometer" models have the slope closest to unity ~~for all years~~ compared to the remaining models, while the first has the lowest variability. Figure~~11 then~~ 11 attempts to evaluate the uncertainty by individually calculating the slope correction factor for each year ~~of the 7 years available~~ from 2018 to 2024 (inclusive) and adjusting the expected accumulated damage of the two best performing virtual load sensors by the average slope $\eta_{avg} = 1/N \cdot \sum_k^N \eta_k$ ~~,~~ (where N is the number of years~~. According to Schillaci (2022), to reach an estimate ~~) and the annual slope variability with the~~ standard deviation (std) and minimum/maximum values. The slope variability could be driven by annual wind statistics and model performances (see Figure 8). To reach an estimate std accuracy of $\pm 10\%$ with limited samples with confidence 90%, more than 100 samples are required, considering a Gaussian distribution (Schillaci, 2022). Since our available N is low (7 years), both the ~~(std)~~ std and the maximum/minimum bounds are evaluated.

~~(a) Comparison between accumulated damage from virtual load sensors ($D_{T,vls}$) and measured ($D_{T,m}$) for 2018. The slope η_k of each model refers to the linear fit slope, while "R^{2}" refers to the coefficient of determination (markers are shown once per month). (b) The slope η_k calculated for each full year $_k$. Blue for NlaggedFNN and orange for LSTM. Measured $D_{T,m}$ and adjusted $D_{T,a}$ damage accumulation of the virtual load sensors based on the yearly slope correction are shown. Only the two best performing models are shown. The adjusted damage by the average slope value for the 8 years is shown as the markers. The filled areas represent the variation around the standard deviation (inner) and bounded between the maximum and minimum possible values observed (outer). The error between virtual load sensor and measured damages accumulation in shown on the right red y-axis. It can be said that the~~ The model "All" with LSTM has the shortest error convergence time nearly within 6 months, and has a mean error for the adjusted accumulated damage equal to -1.8% and variability within 3.5% and -6.5%. The second best performing model "SCADA + Accelerometer" with LSTM has a mean error of -4.2% and a variability bounded within 13% and -15%. The remaining virtual load sensors are ~~also shown, but should not be considered as reliable as the latter, since these do not capture neither the PSD nor the stress ranges~~ not shown since they capture the PSD and the stress

range distribution in a less consistent manner. ~~In other words, the final damage will match but with a very different estimated $M_{fore-aft}$ signal compared to the measured.~~

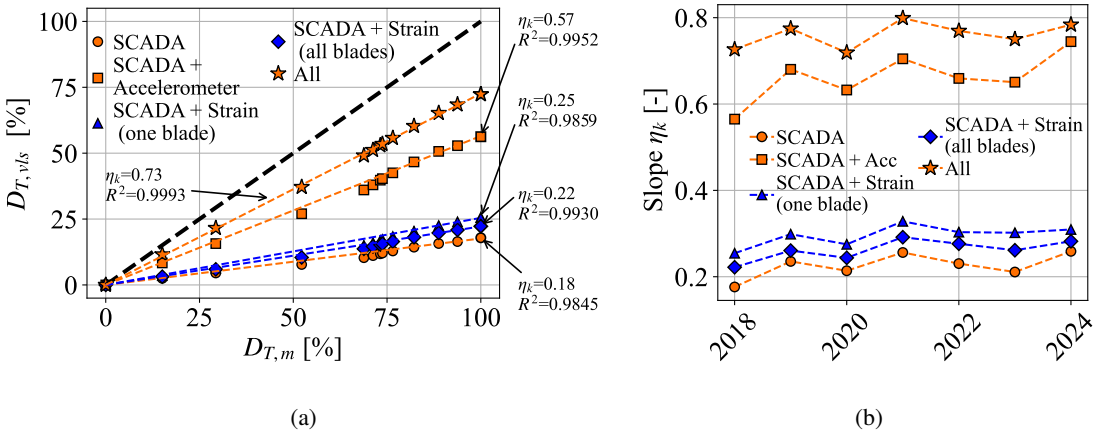

Figure 10. (a) Comparison between accumulated damage from virtual load sensors ($D_{T,vls}$) and measured ($D_{T,m}$) for 2018. The slope η_k of each model refers to the linear fit slope, while "R^2" refers to the coefficient of determination (markers are shown once per month). (b) The slope η_k calculated for each full year $_k$. Blue for NlaggedFNN and orange for LSTM.

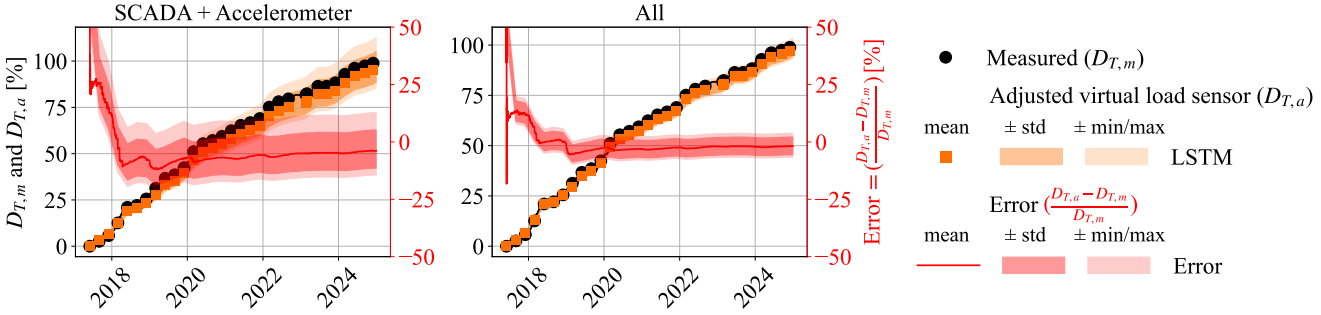

Figure 11. Measured $D_{T,m}$ and adjusted $D_{T,a}$ damage accumulation of the virtual load sensors based on the yearly slope correction are shown. The two best performing models are shown. The adjusted damage by the average slope value from 2018 to 2024 (inclusive) is shown as the markers. The filled areas represent the variation around the standard deviation (inner) and bounded between maximum and minimum values observed (outer). The error between virtual load sensor and measured damage accumulation in shown on the right red y-axis.

The experimental slope correction results should not be seen as fully validated, but as a trial to adjust models that consistently capture the dynamic content of the tower bottom while underpredicting the peaks and valleys, leading to stress range underprediction.

5.5 Main bearings loads and fatigue lifetime analysis

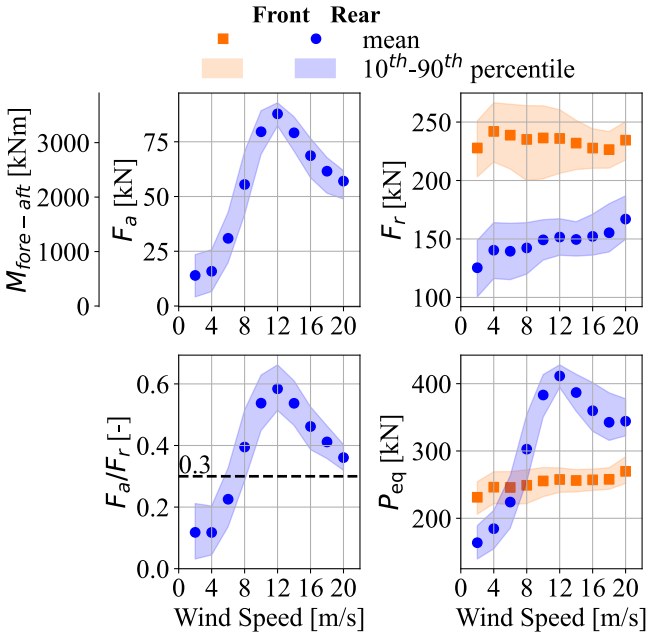

Figure 12. Front and rear main bearing loads as function of the wind speed. The obtained axial load F_a radial as function of the tower bottom bending moment $M_{fore-aft}$, the radial load F_r, the ratio with the rear bearing limiting factor, and the dynamic equivalent load P_{eq} are presented. Mean value is represented by the marker while the 10^{th}-90^{th} percentiles by the filled area from 2016 to 2024 (inclusive).

As detailed in Section 2.2, the main bearing life is calculated directly from the applied radial and axial loads. The axial load of the main bearing F_a is linearly linked to the tower bottom bending moment as in $F_a = M_{fore-aft}/h$, where h is the height difference between hub height (44 m) and the height of the sensor (3.787 m). Here, $M_{fore-aft}$ is assumed to be representative of the turbine thrust curve. The radial load of the main bearings F_r is equal to the estimated ~~R_f~~ $F_{r,f}$ (front) and ~~R_r~~ $F_{r,r}$ (rear), respectively. For a more detailed explanation, see Sections 3 and 4.2. The ~~10-min~~ 10 min mean loads are shown in Figure 12 as a function of wind speed. The front and rear bearings F_r have different behavior with respect to the wind speed. The front main bearing has a fairly flat distribution at higher load, while, for the rear main bearing, the radial load ~~is incremental~~incrementally increases. The F_a/F_r ratio for the rear main bearing is almost in its entirety above the limiting factor, which will worsen the estimated rating life, as the Y factor increases (see Equation 4). Finally, P_{eq} of the front bearing has a slight positive trend, most probably due to higher rotor speeds with higher wind speed, while the rear bearing's dynamic equivalent load is driven by the axial load F_a. A similar analysis shown in Figure 9 was performed for the main bearing fatigue damage, D_B, with the five best virtual load sensors combinations yielding errors below 2%, likely because bearing fatigue is dominated by the mean P_{eq} rather than load fluctuations in the radial F_r and axial F_a loads. Further investigations focus on the tower fatigue damage, D_T.

~~Front and rear main bearing loads as function of the wind speed. The obtained axial load F_a radial as function of the tower bottom bending moment $M_{fore-aft}$, the radial load F_r, the ratio with the rear bearing limiting factor, and the dynamic equivalent load P_{eq} are presented. The 9 years mean value is represented by the marker while the 10^{th}-90^{th} percentiles by the filled area.~~

5.5.1 Sampling frequency and gearbox mounting stiffness assumptions

Before moving on to the long-term results, it is important to verify some of the assumptions made in this work. As in the fatigue estimation of the tower bottom, the P_{eq} and ~~the~~ L_{10} were calculated based on a ~~downsampling of the measured data~~ measured data downsampled from 50 to 10 Hz. ~~Figure 13 shows the effect of this assumption on the estimated loads, as the variation from the estimated downsampled load less the measured load at 50 Hz(normalized). It seems fair to conclude that at 10Hz~~At 10 Hz, there will be a mean error of less than 2% with a 10^{th}-90^{th} ~~, within~~percentile within 5%.

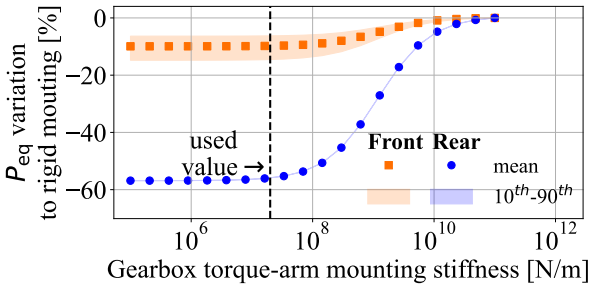

Figure 13. Results of sensitivity analysis of ~~160 h data~~ the stiffness of gearbox mounts on the main bearings dynamic equivalent load P_{eq} ~~; left: influence of sampling frequency of measurements; right: influence of stiffness of gearbox mounts~~based on 160 h randomly selected dataset. The used value (black dashed line) for the gearbox mounting stiffness refers to a stiffness of $20{\cdot}10^6$ [N/m], close to the literature values found in Haastrup et al. (2011) and Keller et al. (2016).

~~On the other hand, the assumption on which stiffness should be~~ Figure 13 shows the effect of the stiffness used to model the gearbox mounting fixation points ~~into the bedplate has been shown to be one order of magnitude more relevant. In the right subplot of~~ on the P_{eq} of the front and rear main bearing. Small variation is observed if the stiffness is neglected or used as in the literature (Haastrup et al., 2011; Keller et al., 2016). However, as shown in Figure 13, ~~nearly~~ an overprediction of 10% and 60% ~~overprediction~~ of the front and rear dynamic equivalent loads P_{eq} could be reached ~~,~~ if a gearbox is ~~assumed to be~~ rigidly fixed in a 4-point drivetrain, ~~see Figure 3~~which is not a realistic assumption.

5.5.2 Environmental and operational conditions (EOCs) mapping of the main bearings dynamic equivalent loads P_{eq}

~~Having 7.5 years of the~~ The main bearing P_{eq} ~~available, it was possible to couple such values~~ was mapped with the environmental conditions of each mean 10 min instance to visualize potential patterns. Figure 14 confirms the intuitive reasoning that the equivalent loads of the front main bearing $P_{eq,f}$ are driven more by the static gravitational load of the rotor. However, $P_{eq,f}$

still contains almost 10% fluctuations due to the shear exponent from 0.05 to 0.15 in all wind ranges and a similar turbulence effect at the rated wind speed. In a different manner, for the rear main bearing, the turbine thrust curve dictates the value of $P_{eq,r}$.

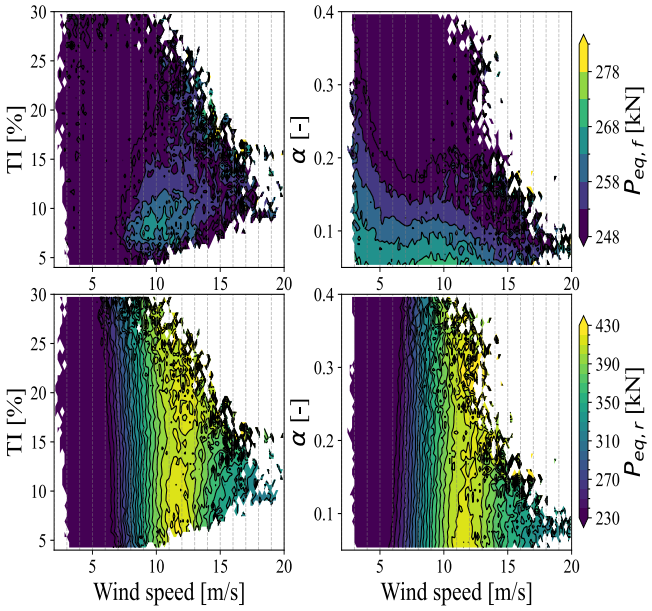

Figure 14. Equivalent dynamic loads of the front ~~(~~$P_{eq,f}$ (top) and rear ~~(~~$P_{eq,r}$ (bottom) main ~~bearing~~ bearings of the DTU research V52 turbine mapped as function of wind speed, turbulence intensity TI and shear exponent α. The measurement period covers from ~~July~~ 2016 to ~~July~~ 2024 (~~included~~inclusive).

Looking closely at $P_{eq,f}$, the results ~~fairly~~ resemble Kenworthy et al. (2024) for a 3-point ~~drive train~~ drivetrain for the effect of lower shear on increased bearing loads. ~~However, a more substantial~~ A comparable effect of low turbulence is found at the rated wind speed~~, which is comparable and can exceed the shear influence, as also suggested by the HIPERWIND D5.4 (2024) report~~. An increase of 10% of $P_{eq,f}$ loads (from 248 to 268 kNm) can be seen in the rated wind speed for the turbulence values of 15% to 10%. A similar load increase is observed for shear exponents of 0.15 to 0.08 at rated wind.

In terms of the load on the rear main bearing $P_{eq,r}$ (locating), ~~in addition to the dominant influence of the mean wind speed in general, the effects of turbulence are similar to the main front bearing at the rated wind speed~~low turbulence can exceed the shear influence at rated wind speed, as also suggested by the HIPERWIND D5.4 (2024) report. This is a result of keeping the level of axial load F_a at the peak of the thrust curve. Approximately 10% increase in load driven by a change in turbulence from 15% to 8%. ~~Although shear also has an influence on loads, it is to a lesser extent.~~

~~Important to note, the discussion above does not imply an overall longer or shorter~~ The peak of the thrust curve is claimed to be the main driver of the fatigue load in the locating bearing $P_{eq,r}$ (Kenworthy et al., 2024; Quick et al.). However, Figure 14 highlights the effect of the low turbulence intensity at the rated wind speed, referring to the most damaging operating condition mapped, and that should affect the lifetime of the main bearing ~~, as Figure 14 zooms in on the most damaging environmental~~

~~combinations and disregards, for example, the effect of shear and turbulenceat smaller loads, as the color bar was limited to focus on higher loads (50^{th} percentile minimum). The goal is to discuss possible load reductions in the case of more damaging conditions.~~

5.5.3 ~~Main bearing lifetime using thrust estimate from virtual load sensors~~

~~The application of virtual load sensors as a thrust estimate and then the~~ more severely depending on the probability of occurrence, as described in Equation 6. To explain this observation, Figure 15 shows a simplified representation of the increase in fatigue load of a locating main bearing at low turbulence. Wind speed is defined as a normal distribution with a mean value at rated U_{rated}, the peak of the thrust curve, and a standard deviation σ defined by $TI = \sigma / U_{rated}$. The dynamic load P is calculated according to Equation 4 and the axial load F_a has been replaced by a scaled thrust curve of a reference wind turbine (Bak et al., 2013) in order to have a complete curve below and above rated conditions. A decrease from 20% to 10% in TI in the wind speed distribution increased the mean dynamic load $\bar{P}$ of the rear main bearing ~~resulted, for all models, in an estimation error of $L_{10,r}$ around~~ in the DTU research V52 turbine by nearly 10%~~for 7.5 years. The model with only "SCADA" with LSTM was the best performing model. This might come from the fact that the main bearing loads, and, consequently, their useful life, are not affected by the dynamic component of the axial load , but only by the mean load level. In this manner, there was no significant performance difference between deploying the different virtual load sensors, in agreement with the results in Figure 7(e).~~ . Similar results were observed for $P_{eq,r}$ in Figure 14. This effect arises from the turbulence averaging of the dynamic load P, as expressed in the following equation.

$$\bar{P} = \int p_N(U) \cdot P(U) dU \tag{20}$$

where $\bar{P}$ is the mean of the dynamic load P, p_N is the normal distribution that represents the wind speed, and $P(U)$ is the dynamic load P as a function of the wind speed U.

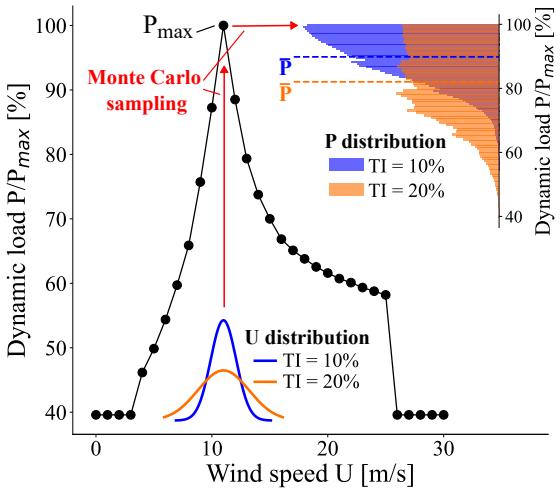

Figure 15. Conceptual representation of the effect of turbulence intensity TI at rated wind speed on the wind speed distribution U, modeled as a normal distribution (see bottom inset), and its influence on the dynamic load P distribution on the rear main bearing of the DTU research V52 turbine (see top right inset). In this simple exercise, the turbine thrust values are derived from a simplified DTU 10 MW (Bak et al., 2013) thrust curve scaled to the DTU research V52 turbine by the maximum axial load F_a, as shown in Figure 12, in order to generate a representative and complete thrust curve. A Monte Carlo sampling is used with 10^6 samples to generate the P histogram. The numerically obtained mean dynamic load $\bar{P}$ can also be calculated using Equation 20 at rated wind speed and is shown as horizontal dashed lines.

5.5.3 ~~Main bearings modified rating life: L_{10m} and a_{ISO}~~

5.5.3 Main bearings L_{10m} and a_{ISO}

Applying the drivetrain thermal model, consistent temperature ranges were found for the normal operating conditions (DLC 1.2) of the main bearings. The temperatures of the front and rear main bearings had minimum/mean/maximum values of 8/34/55~~and~~ °C and 18/40/61°C, respectively, while the viscosity ratio κ ~~(viscosity ratio)~~ had minimum values of 0.84 and 0.64~~respectively.~~, respectively. The gearbox temperature model yielded 3 °C MAE, which is reasonable considering the scope of this investigation.

~~The modified rating life of the front $L_{10m,f}$ and rear $L_{10m,r}$ main bearings of the DTU research V52 turbine is mapped as function of relevant environmental conditions. It is assumed a severe level of contamination for the grease lubricant. The latter represents a scenario in which re-greasing intervals recommended by the OEM are not followed. Important to note that there are limits related to a_{ISO} implementation as defined by ISO-281 (2007): at $a_{\mathrm{ISO}} = 50$ and at $e_c C_u / P_{eq} = 5$ (maximum bound) and at viscosity ratio $\kappa = 0.1$ (minimum bound) which has not been reached in this work. The lower limit of the color bar (yellow color) was chosen to match the turbine design lifetime of 20 years. The measurement period covers from July 2016 to July 2024 (included).~~ The seasonal variation corresponded to approximately ±10°C in the front bearing and ±8 °C in the rear bearing

temperatures, while the operational variability reached around ±15°C variation in the front and ±20°C in the rear bearing temperatures. The results of such environmental and operation conditions (EOCs) can be visualized in Figure 16, assuming a severe level of grease contamination. The grease cleanliness affects the parameters to estimate the variable contamination factor e_c, which by consequence affects the a_{ISO} ~~(see ISO-281 (2007))~~(ISO-281, 2007). This assumption represents a worse scenario in which re-greasing of the main bearings is not performed in the long-term as suggested by the manufactures. ~~It~~ Figure 16 highlights the large impact of the ambient temperature on the modified rating lifetimes of main bearings in which there is no nacelle temperature control. For the rear main bearing, even for such an overdesigned bearing, at rated wind speed ~~and~~ with low TI or with ambient temperatures above 20°C, the bearing lifetime is reduced to below the design lifetime of 20 years. In addition to that, once a_{ISO} is considered, it seems that turbulence overcomes shear as the most influential factor for the rear main bearing at the rated wind speed.

~~Even though significant~~

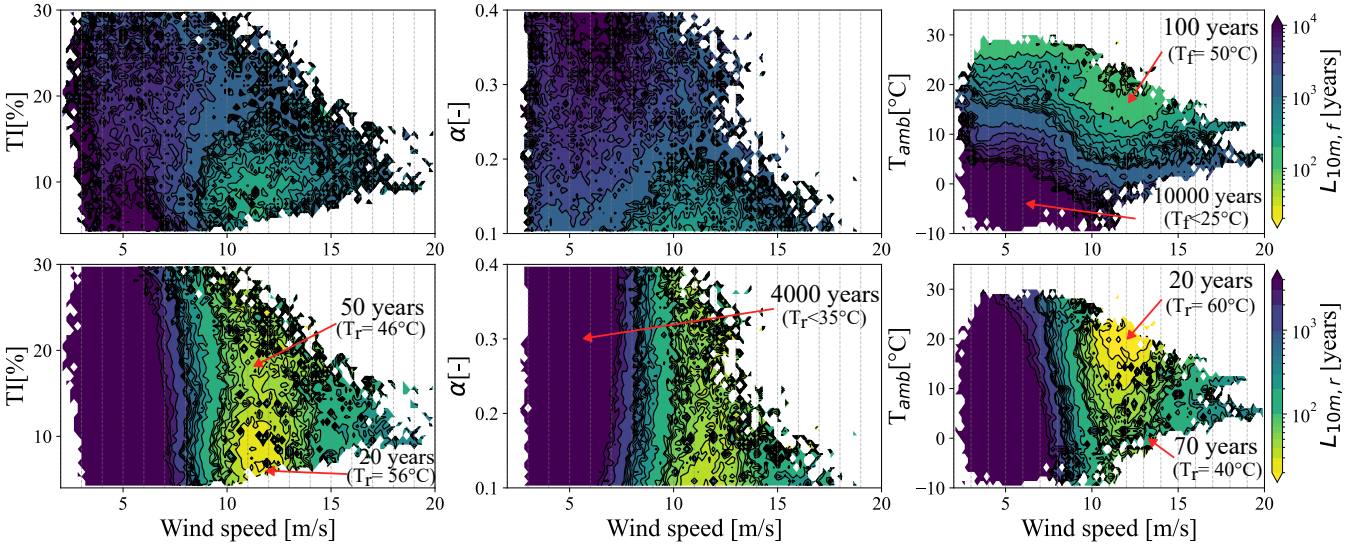

Figure 16. The modified rating life of the front $L_{10m,f}$ (top) and rear $L_{10m,r}$ (bottom) main bearings of the DTU research V52 turbine as function of wind speed, turbulence intensity TI, shear exponent α, and ambient temperature T_{amb}, together with pointers to the rear T_r and front T_f main bearing temperatures. It is assumed a severe level of contamination for the grease lubricant. The latter represents a scenario in which re-greasing intervals recommended by the OEM are not followed. Important to note that there are limits related to a_{ISO} implementation as defined by ISO-281 (2007): at $a_{\mathrm{ISO}} = 50$ and at $e_c C_u / P_{eq} = 5$ (maximum bound) and at viscosity ratio $\kappa = 0.1$ (minimum bound) which has not been reached in this work. The lower limit of the color bar (yellow color) was chosen to match the turbine design lifetime of 20 years.

Significant variations can be observed on the L_{10m} due to EOCs, but it is important to mention that the grease cleanliness level ~~affects~~ should affect the bearing lifetime more severely ~~. A severe level of contamination could be reached at the end of the design lifetime in case no periodic re-greasing are carried out, as described by ISO-281 (2007). However, there are better and worse scenarios.~~ (Kenworthy et al., 2024). Figure 17 shows ~~in a log~~ on a logarithmic scale the distribution of a_{ISO} as a function

of the grease cleanliness assumed or inspected in a wind turbine. In the worst case scenario with "very severe contamination" ~~around~~ 70% of instances are penalized and ~~$L_{10m,r}$ goes from the initial $L_{10,r}$ of 315 years to 130 years lifetime, more than 50% lifetime reduction.~~

$L_{10,r} = 566$ years goes to $L_{10m,r} = 200$ years lifetime.

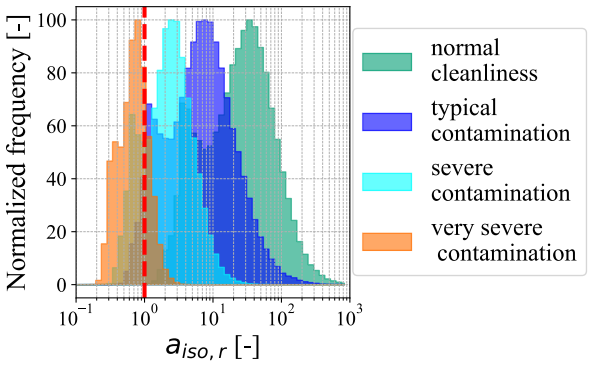

Figure 17. Normalized histogram showing the distribution of the rear main bearing life modification factor $a_{ISO,r}$ as function of the grease cleanliness levels. The red dashed line shows the limit for ~~$L_{10} = L_{10,m}$~~ $L_{10} = L_{10m}$. The bound of $a_{ISO} < 50$ is not applied for the sake of clarity.

6 ~~Discussion~~

~~The assumption that the strain gauge zero-drift in a wind turbine tower and blade follows a linear curve might be an oversimplification. Many factors can influence the zero drift of the strain gauges. As described by Hoffmann (1989), the measuring grid has its own fatigue deterioration, the adhesive can wear over time, and the bending of the connecting wires and several impurities (e.g., mold) that can add unwanted electrical resistance to the circuit over time. However, it is interesting to observe that eight independent strain gauges from the DTU research V52 turbine have presented similar behavior over time, with low unexplained variability after the proposed correction. Similar variability was also found for a 5 MW offshore turbine in Faria et al. (2025) . The larger variability from the blade root strain gauges calibration factors could be explained by the fact that its Wheatstone bridge is compensated for temperature differences in the whole blade, but not for temperature gradients between the two blade surfaces. It would be interesting to see if this result holds in more case studies.~~

~~One last detail worth mentioning about the strain gauge methodology is that the configuration of the Wheatstone bridge chosen to measure bending moments will highly affect the reliability of the sensors output. The full bridge of the blade root strain gauges was not inherently compensated for temperature gradients between the blade faces, differently from the full-bridge of the tower bottom strain gauges. Because of that, the residuals had a small seasonality effect present. So, temperature effects can also add variability and bias to the zero drift of strain gauges.~~

In terms of virtual load sensors, it was a methodological decision to use k-means to select and generate training and validation datasets. Rather than a more generalizable conclusion usually sought by methods such as the Latin-Hyper cube, the goal here was to test and deploy the best-performing model for the long-term monitoring of the DTU research V52 turbine, as it is rare to find similar results in the literature. The performance of the virtual load sensor for DEL estimation is worse than that found in works such as de N Santos et al. (2024). The addition from the present work comes from the deployment of long-term and time series virtual load sensor. In which it is interesting to highlight that a mere 1% difference in MAE DEL between models led to a 11% difference in the lifetime estimation. The experimental slope correction results should not be seen as fully validated, but as a trial to adjust models that consistently capture the dynamic content of the tower bottom while underpredicting the peaks and valleys, leading to constant stress range underprediction. Using in this work 7 years of measurements showed very low variability, within around ± 5 % for the best performing model (LSTM with "All" inputs). More advances in machine learning models and training techniques could still be tried.

Regarding monitoring the bearing lifetime, it was interesting to observe that the initial gearbox assumption could lead to large errors in the estimation of the lifetime of the components. The stiffness of the gearbox mounting could lead to an error of 60% P_{eq}, which, due to the bearing exponent p equal to $10/3$, would mean underestimating the lifetime L_{10} by 198% for the location of the main bearing.

The lifetime estimate of the main bearings was an order of magnitude higher than the required lifetime of 20 years, making it less probable to fail due to rolling contact fatigue in the DTU research V52 turbine. However, mapping of their loads facing key environmental conditions can provide more generalizable lessons on how to operate and maintain such expensive components in the long term for other turbines with similar drivetrain setup. At a wind farm level, if farm power curtailment is required, turbines with low inflow turbulence could be prioritized to be curtailed to have a more significant reduction of main bearing loads. In contrast to what one would intuitively expect in the field of wind energy research, lower intensities of turbulence could penalize the useful life of the main bearings, as also shown in HIPERWIND D5.4 (2024). In fact, good estimates of operating temperature and grease cleanliness were identified as key drivers in the estimation of main bearings lifetime. Although the thermal model resulted in realistic temperature ranges, validation with measurement values is the logical next step.

6 Conclusion

In this work, methods were investigated to allow for reliable lifetime counting of large load-carrying components, both structural in the form of a tower and rotating in the form of main bearings. The work was validated on the DTU research V52 wind turbine for a continuous period of almost a decade.

From the proposed research questions that guided this study, the main learnings and possible limitations are as follows.

The strain gauges at the bottom of the tower and the root of the blade were continual calibrated for 9.5 years continually calibrated from 2016 to 2024 (inclusive) with at least 20 calibration instances per year. The yaw sweeps and Low-Speed Idling (LSI) routines were verified for long-term calibration, and all strain gauges presented reliable behavior. We assumed linear behavior to model the zero drift of the strain gauges, which has to be validated by carrying larger case-study comparisons

. accounting for different Wheatstone bridge configurations. However, it is interesting to observe that eight full strain gauge bridges from the DTU research V52 turbine have presented similar behavior over time, with low unexplained variability after the proposed correction.

Lifetime counting of a structural component, such as the tower, and other load-carrying components, such as main bearings, was carried out for almost a decade, without having design information from the blade or mid-fidelity aeroelastic models in hands. Attention should be paid to the quality of SCADA sensors and drivetrain modeling assumptions. .

The use of virtual load sensors based on data-driven methods is promising in the field of wind energy, where Structural Health Monitoring (SHM) campaigns can be expensive and take a long time (even more for offshore assets). These could serve as a continuous high-frequency thrust estimate. In this work, the counting of counting 7.5 years of the fatigue lifetime of the tower bottom using a virtual load sensor yielded in its best model a prediction of damage of a damage prediction of 75% , and after of the best performing model. It is interesting to highlight that a 1% difference in MAE DEL between models with and without blade root strain gauges resulted in a 11% difference in the lifetime estimation. After an experimental correction, assuming a year of available measurement data, the lifetime error was reduced to $\pm 5\%$ lifetime error. However, in the field of . Future research could investigate minimum measurement periods for a reliable slope correction, assumptions on the training of the data-driven methodologies, there are many models, training techniques, and deployment models, such as clustering K-means and the error function (de N Santos et al., 2024), and test cases that could bias the results. For this reason, the analysis. The results from this work might not be seen as the considered state of the art or entirely generalizable but but be seen as a discussion on of the challenges of applying and validating long-term and continuous deploying of virtual load sensors on operating in wind turbines considering several DLCs. DLCs.

Finally, the main bearings loads P_{eq} and modified lifetime $L_{10,m}$ L_{10m} were mapped in terms of relevant environmental conditions and grease cleanliness. The first showed that a front main bearing in a 4-point drivetrain has longer life by a higher shear exponent a longer life as the shear exponent increases, whereas the fatigue loads in the locating rear main bearing , are dictated by the peak of the thrust curve and are larger at rated wind speed, has higher loads for lower turbulence intensities. Neglecting the stiffness of the gearbox mount renders unrealistically high P_{eq}, but having the stiffness values within realistic ranges results in little influence on the lifetime. Finally, ISO-281 (2007) life corrections for lubricant cleanliness result in significantly different lifetimes but are not . The rear main bearing was observed to have a longer lifetime as the shear and turbulence intensity increase, which can be explained by the turbulence averaging of the thrust loads. Estimates of operating temperature and grease cleanliness (Kenworthy et al., 2024) were identified as key drivers in the modified rating lifetime L_{10m} of the main bearings. Although the drivetrain thermal model resulted in realistic temperature ranges, validation with measurement values is the logical next step. Lubricant cleanliness corrections significantly affect predicted lifetime but have not been validated for large grease-lubricated bearings. Future research might focus on establishing these factors with bearings and lubricants typically used in wind turbines, unlike smaller bearings (Needelman and Zaretsky, 2014).

Appendix A: Azimuth angle correction for the DTU research V52 turbine

Figure A1 presents the problem and the solution applied for the azimuth angle sensor. For periods before 2018 and after 2020, the measured azimuth angles contained severe variations in regular patterns, which did not extend to variability in the edgewise bending moment $M_{edgewise}$ of the blades. In this manner, such variations were triggered as a sensor malfunctioning.

To correct for such an issue, an azimuth angle estimate φ_e was derived as a constant-gain blend between two complementary signals. The first signal is the measured azimuth angle φ_m sampled at 10 Hz, shown in Figure A1 as the black line (left y-axis). The second signal is the controller-defined rotor speed (SCADA) ω sampled at 10 Hz, which has a lower resolution, and shown in the same figure as the red line (right y-axis). The period Δt is defined as the inverse of the sampling frequency.

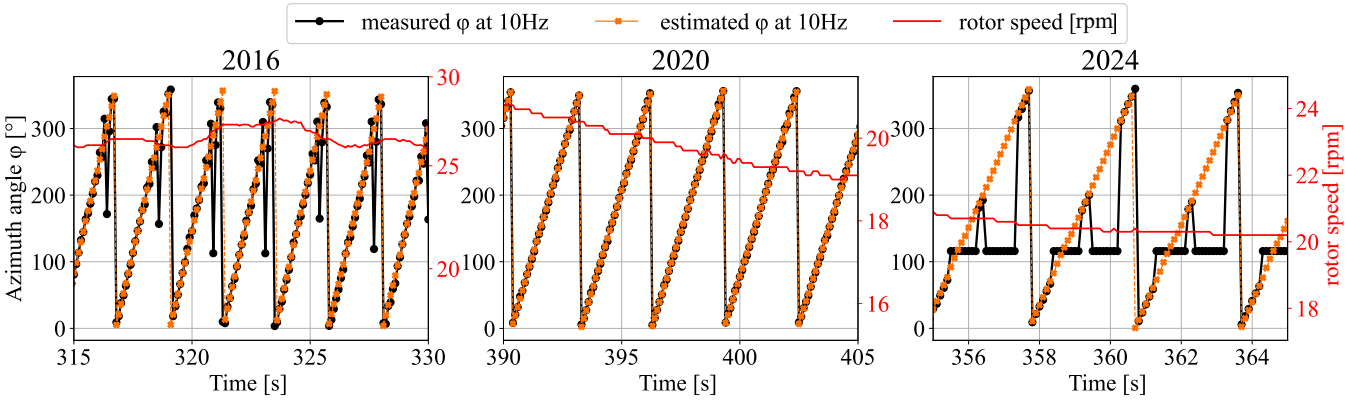

Figure A1. Representative examples of the azimuth angle in the SCADA from the DTU research V52 turbine showing problems with the measurement data acquired in 2016 and 2024. An estimated azimuth angle (orange) is performed based on the controller SCADA rotor speed (red) and the measured azimuth angle (black).

The correction method works by first identifying the best phase shift $\varphi_{r,0}$ of the azimuth angle in a 10 min instance, which is the initial point between the cumulative φ_m and $\sum_i \omega_i \cdot \Delta t$, using a few sequential data points. The instantaneous angle based on the rotor speed will be $\varphi_{r,i} = \omega_i \cdot \Delta t + \varphi_{r,i-1}$, for $i > 1$, and $\varphi_{r,i} = \varphi_{r,0}$, for $i = 1$. The final estimated azimuth is defined as $\varphi_{e,i} = \varphi_{r,i} + K \cdot d$, if $d < d_{limit}$ and $\gamma_{e,i} = \varphi_{r,i}$, if $d > d_{limit}$. In which, d is the difference between the measured instantaneous angle and the estimation of the rotor speed $d = \varphi_{m,i} - \varphi_{r,i}$. The two manually tuned variables are the gain K and the distance limit d_{limit}. The first defines how reliable are the fluctuations from the measured azimuth. The latter correlates with the threshold of how many degrees the measured azimuth can realistically change within Δt. In this work, the parameters were tuned to $K = 0.1$ and $d_{limit} = 30°$.

The validation was carried out in a good year (2019) by applying the method on 160 h of representative instances containing the Design Load Cases (DLC) 1.2, 3.1 and 4.1. The maximum instantaneous error $/\varphi_m - \varphi_e/$ was below 5°.

Appendix B: Statically indeterminate system ~~of equations~~ for a 4-point drivetrain considering ~~a~~ the gearbox mounting stiffness

Figure B1 shows the drivetrain schematic that allows one to derive the radial loads in the main bearings while considering the stiffness of the gearbox mounting, as shown in Figure 3a. The vertical direction is chosen as it includes the most significant resultant loads (gravitational and aerodynamic), and the horizontal direction can be solved in the same manner. The static gravitational loads acting on the main shaft are derived from a combination of public sources and visual inspections of the turbine nacelle. Similar for lengths (e.g. L_{shaft}). The gravitational force of the rotor F_{rotor} is calculated assuming a rotor and a hub mass of 10 tons (third party source, see Scribd (2021)). The gravitational force of the shaft F_{shaft} assumes a shaft mass equal to 1 ton, between an internal estimate of 0.8 tons and the Fingersh et al. (2006) estimate of 1.2 tons, which uses the best-fit equation $m_{shaft} = 0.0142 \cdot D^{2.888}$ from historical data (given D as the rotor diameter in meters and the mass in tons).

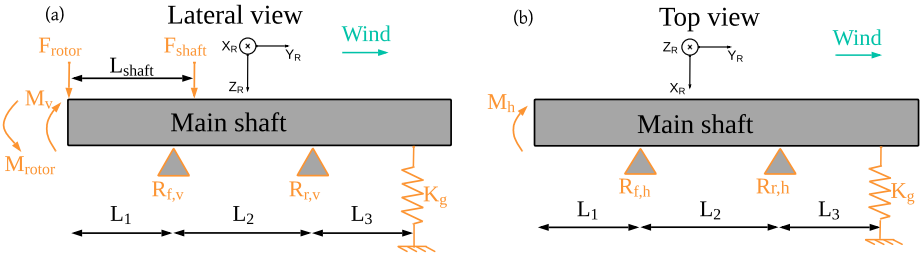

Figure B1. Drivetrain schematic used to represent the external loads applied and the supporting elements in the ~~vertical direction~~(a) lateral view and (b) top view, in respect to the rotor coordinate system XYZ_R. F_{rotor} and F_{shaft} are the rotor and shaft gravitational loads respectively, L_{shaft} the shaft center of mass distance, M_{rotor} the bending resultant from the rotor weight F_{rotor} and L_{hub} as the hub is not modeled (see Figure 3), and $M_{~~v~~}$ is the aerodynamical loading at the vertical direction. The main shaft is supported by the front $R_{~~f,v~~f}$ and rear $R_{~~r,v~~r}$ main bearings (refereed in the main text as $F_{r,f}$ and $F_{r,r}$), in the vertical v and horizontal h directions. Lastly, it is supported by the gearbox through the equivalent spring K_g, which results in the force F_g.

The system of equations for the forces and bending moments for Figure B1a is composed of:

$$\sum F = 0 = -F_{rotor} - F_{shaft} + R_{f,vf} + R_{r,vr} + F_g \tag{B1}$$

$$\sum M(x=0) = 0 = -M_v + M_{rotor} + R_{f,vf} L_1 - F_{shaft} L_{shaft} + R_{r,vr}(L_1 + L_2) + F_g(L_1 + L_2 + L_3) \tag{B2}$$

where the assumed sign conversion is upwards and anticlockwise as positive. The "Top view" (Figure B1b) has the same formulation, it is solved independently, but without gravitational loads F_{rotor}, M_{rotor} and F_{shaft}.

Since the system is statically indeterminate, there are two independent equations B1 and B2 and 3 unknowns reactions $R_{~~f,v~~}$, $R_{~~r,v~~f}$, R_r and F_g. To add a third equation, the main shaft is modeled as a flexible beam, with small deflections, linear material ~~, and~~ (young modulus E) and second area moment of inertia I ~~constants~~ along the length, as explained by Budynas and Nisbett (2020).

~~The following equations are used to describe~~ Equation B4 describes the bending moment as a function of ~~x and the~~ beam deflection w along x through a double integration step.

$$EI\frac{d^2w}{dx^2} = M = -M_v + M_{rotor} + F_{rotor}\cdot x + F_{shaft}\cdot\langle x - L_{shaft}\rangle - R_{f,v}\cdot\langle x - L_1\rangle - R_{r,v}\cdot\langle x - (L_1+L_2)\rangle \tag{B3}$$

$$\begin{aligned} EIw = &-\frac{M_v}{2}\cdot x^2 + \frac{M_{rotor}}{2}\cdot x^2 + \frac{F_{rotor}}{6}\cdot x^3 + \frac{F_{shaft}}{6}\cdot\langle x - L_{shaft}\rangle^3 \\ &-\frac{R_{f,v}}{6}\cdot\langle x - L_1\rangle^3 - \frac{R_{r,v}}{6}\cdot\langle x - (L_1+L_2)\rangle^3 + C_1\cdot x + C_2 \end{aligned} \tag{B4}$$

where $\langle\rangle$ is the Macaulay bracket or discontinuity function. To solve the constants C_1 and C_2, ~~two~~ and generate a third independent equation, three known boundary conditions ~~(deflection at the main bearings)~~ can be used as such:

$$w(x = L_1) = 0 \qquad and\, w(x = L_1 + L_2) = 0 \qquad w(x = L_1 + L_2 + L_3) = \frac{F_g}{K_g} \tag{B5}$$

Finally, once the constants are calculated, the third independent equation can be derived by applying a third known boundary condition (deflection at the gearbox ~~):~~

$$w(x = L_1 + L_2 + L_3) = \frac{F_g}{K_g}$$

F_g/K_g). The resultant third independent equation is then:

$$\begin{aligned} EI\frac{F_g}{K_g} = &-\frac{M_v}{2}(L_1+L_2+L_3)^2 + \frac{M_{rotor}}{2}(L_1+L_2+L_3)^2 + \frac{F_{rotor}}{6}(L_1+L_2+L_3)^3 \\ &+\frac{F_{shaft}}{6}(L_1+L_2+L_3-L_{shaft})^3 - \frac{R_{f,v}}{6}\frac{R_f}{6}(L_2+L_3)^3 - \frac{R_{r,v}}{6}\frac{R_r}{6}(L_3)^3 + C_1(L_1+L_2+L_3) + C_2 \end{aligned} \tag{B6}$$

The complete derivation are omitted for conciseness, consisting primarily of algebraic manipulation and variable substitution. Using the three independent equations B1, B2 and B6, and assuming quasi-static equilibrium at each time instant, one can calculate the ~~3~~ independent unknowns $R_{~~f,v~~, ~~R_{r,v}~~}$, R_r and F_g, referred on the main text as $F_{r,f}$, $F_{r,r}$ and F_g.

Appendix C: Hyperparameters tuning of the data-driven virtual load sensors

The models described in Section 4.3 are tuned using a random search tuner (O'Malley et al., 2019) to improve the model performance. Table C1 shows the hyperparameters possible range and optimal value found for each virtual load sensor. Similarly to the methodology applied by Dimitrov and Göçmen (2022) and Gräfe et al. (2024), there are hyperparameters related to the data architecture, such as the number of lags n_{lags} in a NlaggedFNN and the window size in a LSTM, as well as hyperparameters related to the model architecture and training itself. The latter includes, for example, regularization features to improve the model generalization, such as the $L2$ regularizer and dropout. While, the model training was optimized in terms of batch size and learning rate. The range of parameters was similar to that used in Dimitrov and Göçmen (2022).

Table C1. Hyperparameter tuning, including the bound limits and optimum values for each model and feature possible combination.

			Optimal values				
Model	Hyperparameter	Parameter range	SCADA	SCADA + Accelerometer	SCADA + Strain (one blade)	SCADA + Strain (all blade)	All
Feedforward Neural Network (FNN)	Batch size	32:32:256	32	32	160	96	160
	Learning rate	10^{-4}:10^{-2}	$2.5{\cdot}10^{-3}$	$5.8{\cdot}10^{-3}$	$7.2{\cdot}10^{-3}$	$3.0{\cdot}10^{-3}$	$3.5{\cdot}10^{-3}$
	Hidden units	50:20:200	150	190	70	130	150
	L2 regularizer	10^{-6}:10^{-1}	$2.0{\cdot}10^{-6}$	$3.6{\cdot}10^{-6}$	$1.2{\cdot}10^{-6}$	$11.3{\cdot}10^{-6}$	$2.8{\cdot}10^{-6}$
	Second layer	0:1:2	1	1	1	0	0
lagged FNN (NlaggedFNN)	Batch size	32:32:256	32	32	96	96	96
	Learning rate	10^{-4}:10^{-2}	$0.8{\cdot}10^{-3}$	$0.8{\cdot}10^{-3}$	$1.8{\cdot}10^{-3}$	$2.8{\cdot}10^{-3}$	$1.7{\cdot}10^{-3}$
	Hidden units	50:20:200	50	190	150	70	70
	L2 regularizer	10^{-6}:10^{-1}	$1.4{\cdot}10^{-6}$	$1.2{\cdot}10^{-6}$	$4.6{\cdot}10^{-6}$	$1.6{\cdot}10^{-6}$	$5.2{\cdot}10^{-6}$
	Second layer	0:1:3	0	1	0	0	0
	n_{lags}	1:1:6	5	5	6	5	6
Long Short-Term Memory NN (LSTM)	Batch size	32:32:256	128	64	64	64	64
	Learning rate	10^{-4}:10^{-2}	$9.7{\cdot}10^{-3}$	$2.9{\cdot}10^{-3}$	$9.7{\cdot}10^{-3}$	$7.3{\cdot}10^{-3}$	$3.4{\cdot}10^{-3}$
	Window size [s]	2,5,10,30	5	10	5	10	10
	Dropout	0:0.1:0.5	0.1	0.2	0.2	0	0

. BF and AB participated in the conceptualization and design of the work together with DR and XZ. BF performed the measurements processing and conducted the data analysis. BF and ND performed the models training and deployment. BF and NS wrote the draft manuscript. AB, MS, ND and AK supported the results analysis. All reviewed and edited the manuscript.

. Some authors are members of the editorial board of journal Wind Energy Science (WES).

. This work is funded by the Department of Wind and Energy Systems at the Technical University of Denmark (DTU). The university also made the DTU research V52 turbine measurements available. The authors greatly appreciate the support. Special thanks to Steen Arne Sørensen and Søren Oemann Lind for their valuable support with the turbine database and for discussions on the instrumentation. This work has initially received funding from the European Union's Horizon 2020 research and innovation program under grant agreement No 791875 of the ReaLCoE project. The methodology has been inspired by research carried out by the HIPERWIND and the IEA TCP WIND Task 42.

References

ASTM D341-93: Viscosity–Temperature Charts for Liquid Petroleum Products, ASTM Standard ASTM D341-93 (Reapproved 1998), ASTM International, West Conshohocken, PA, USA, an American National Standard., 1998.

ASTM E1049-85: Standard Practices for Cycle Counting in Fatigue Analysis, ASTM Standard ASTM E1049-85 (Reapproved 2017), ASTM International, West Conshohocken, PA, USA, 2017.

Bak, C., Zahle, F., Bitsche, R., Kim, T., Yde, A., Henriksen, L. C., Natarajan, A., and Hansen, M. H.: Description of the DTU 10 MW Reference Wind Turbine, Dtu wind energy report-i-0092, DTU Wind Energy, Technical University of Denmark, Roskilde, Denmark, https://gitlab.windenergy.dtu.dk/rwts/dtu-10mw-rwt/-/raw/master/docs/DTU_Wind_Energy_Report-I-0092.pdf, 2013.

Bengio, Y., Simard, P., and Frasconi, P.: Learning long-term dependencies with gradient descent is difficult, IEEE Transactions on Neural Networks, 5, 157–166, https://doi.org/10.1109/72.279181, 1994.

Budynas, R. G. and Nisbett, J. K.: Shigley's Mechanical Engineering Design, McGraw-Hill Education, New York, NY, 11th edn., professor Emeritus, Kate Gleason College of Engineering, Rochester Institute of Technology; Associate Professor of Mechanical Engineering, Missouri University of Science and Technology, 2020.

D'Antuono, P., Weijtjens, W., and Devriendt, C.: On the Minimum Required Sampling Frequency for Reliable Fatigue Lifetime Estimation in Structural Health Monitoring. How Much is Enough?, in: European Workshop on Structural Health Monitoring, edited by Rizzo, P. and Milazzo, A., pp. 133–142, Springer International Publishing, Cham, ISBN 978-3-031-07254-3, 2023.

de N Santos, F., Noppe, N., Weijtjens, W., and Devriendt, C.: Farm-wide interface fatigue loads estimation: A data-driven approach based on accelerometers, Wind Energy, 27, 321–340, https://doi.org/https://doi.org/10.1002/we.2888, 2024.

Dimitrov, N. and Göçmen, T.: Virtual sensors for wind turbines with machine learning-based time series models, Wind Energy, 25, 1626–1645, https://doi.org/https://doi.org/10.1002/we.2762, 2022.

DNVGL-RP-C203: Fatigue Design of Offshore Steel Structures – Recommended Practice, Edition April 2016, DNVGL RP DNVGL-RP-C203:2016, DNV GL AS, Høvik, Norway, 2016.

Faria, B. R. and Jafaripour, L. Z.: yaw-sweep-sg-cali: Strain-gauge yaw-sweep calibration for wind turbine towers, https://pypi.org/project/yaw-sweep-sg-cali/, version 3.2, 2023.

Faria, B. R., Sadeghi, N., Dimitrov, N., Kolios, A., and Abrahamsen, A. B.: Inclusion of low-frequency cycles on tower fatigue lifetime assessment through relevant environmental and operational conditions, Journal of Physics: Conference Series, 2767, 042 021, https://doi.org/10.1088/1742-6596/2767/4/042021, 2024.

Faria, B. R., Dimitrov, N., Perez, V., Kolios, A., and Abrahamsen, A. B.: Virtual load sensors based on calibrated wind turbine strain sensors for damage accumulation estimation: a gap-filling technique, Journal of Physics: Conference Series, 3025, 012 011, https://doi.org/10.1088/1742-6596/3025/1/012011, 2025.

Fingersh, L., Hand, M., and Laxson, A.: Wind Turbine Design Cost and Scaling Model, Technical Report NREL/TP-500-40566, National Renewable Energy Laboratory (NREL), Golden, CO, USA, https://doi.org/10.2172/897434, 2006.

Gräfe, M., Pettas, V., Dimitrov, N., and Cheng, P. W.: Machine-learning-based virtual load sensors for mooring lines using simulated motion and lidar measurements, Wind Energy Science, 9, 2175–2193, https://doi.org/10.5194/wes-9-2175-2024, 2024.

Haastrup, M., Hansen, M. R., and Ebbesen, M. K.: Modeling of Wind Turbine Gearbox Mounting, Modeling, Identification and Control, 32, 141–149, https://doi.org/10.4173/mic.2011.4.2, 2011.

Hart, E., Clarke, B., Nicholas, G., Kazemi Amiri, A., Stirling, J., Carroll, J., Dwyer-Joyce, R., McDonald, A., and Long, H.: A review of wind turbine main bearings: Design, operation, modelling, damage mechanisms and fault detection, Wind Energy Science, 5, 105–124, https://doi.org/10.5194/WES-5-105-2020, 2020.

Hart, E., Raby, K., Keller, J., Sheng, S., Long, H., Carroll, J., Brasseur, J., and Tough, F.: Main Bearing Replacement and Damage - A Field Data Study on 15 Gigawatts of Wind Energy Capacity, vol. NREL/TP-5000-86228, published by the US National Renewable Energy Laboratory (NREL) as Technical Report NREL/TP-5000-86228, July 2023., 2023.

HIPERWIND D5.1: Component Life Models, Project Deliverable Deliverable D5.1, HIPERWIND Project — HIghly advanced Probabilistic design and Enhanced Reliability methods for high-value, cost-efficient offshore WIND, Lyngby, Denmark, https://www.hiperwind.eu/deliverables-and-publications, 2023.

HIPERWIND D5.4: Development and implementation of probabilistic and uncertainty quantification methods for reliability sensitivity analysi, Project Deliverable Deliverable D5.4, HIPERWIND Project — HIghly advanced Probabilistic design and Enhanced Reliability methods for high-value, cost-efficient offshore WIND, Lyngby, Denmark, https://www.hiperwind.eu/deliverables-and-publications, 2024.

Hoffmann, K.: An Introduction to Measurements Using Strain Gages, Hottinger Baldwin Messtechnik GmbH, Darmstadt, Germany, all rights reserved. © Hottinger Baldwin Messtechnik GmbH, 1989. Reproduction or distribution, in whole or in part, requires express written permission from the publisher., 1989.

Hübler, C. and Rolfes, R.: Probabilistic temporal extrapolation of fatigue damage of offshore wind turbine substructures based on strain measurements, Wind Energy Science, 7, 1919–1940, https://doi.org/10.5194/wes-7-1919-2022, 2022.

IEA and NEA: Projected Costs of Generating Electricity: 2020 Edition, Tech. rep., International Energy Agency and OECD Nuclear Energy Agency, Paris, ISBN 978-92-64-55471-9, https://doi.org/10.1787/a6002f3b-en, 2020.

IEC 61400-1: Wind energy generation systems – Part 1: Design requirements, Edition 4, IEC 61400-1:2019, International Electrotechnical Commission, Geneva, Switzerland, 2019.

IEC 61400-13: Wind energy generation systems – Part 13: Measurement of mechanical loads, IEC 61400-13:2016, International Electrotechnical Commission, Geneva, Switzerland, 2016.

IEC-TS-61400-28: Wind energy generation systems — Part 28: Through life management and life extension of wind power assets, IEC TS 61400-28:2020, International Electrotechnical Commission, Geneva, Switzerland, 2020.

IRENA: Renewable Power Generation Costs in 2023, Tech. rep., International Renewable Energy Agency, Abu Dhabi, ISBN 978-92-9260-621-3, https://www.irena.org/Publications/2024/Sep/Renewable-Power-Generation-Costs-in-2023, 2024.

ISO-281: Rolling bearings — Dynamic load ratings and rating life, ISO 281:2007, International Organization for Standardization, Geneva, Switzerland, 2007.

Keller, J., Guo, Y., and Sethuraman, L.: Gearbox Reliability Collaborative: Investigation of Gearbox Motion and High-Speed-Shaft Loads, Technical Report NREL/TP-5000-65321, National Renewable Energy Laboratory (NREL), Golden, CO, USA, https://doi.org/10.2172/1243302, 2016.

Kenworthy, J., Hart, E., Stirling, J., Stock, A., Keller, J., Guo, Y., Brasseur, J., and Evans, R.: Wind turbine main bearing rating lives as determined by IEC 61400-1 and ISO 281: A critical review and exploratory case study, Wind Energy, 27, 179–197, https://doi.org/https://doi.org/10.1002/we.2883, 2024.

Loraux, C. and Brühwiler, E.: The use of long term monitoring data for the extension of the service duration of existing wind turbine support structures, Journal of Physics: Conference Series, 753, 072 023, https://doi.org/10.1088/1742-6596/753/7/072023, 2016.

Mehlan, F. C., Keller, J., and Nejad, A. R.: Virtual sensing of wind turbine hub loads and drivetrain fatigue damage, Forschung im Ingenieurwesen, 87, 207–218, https://doi.org/https://doi.org/10.1007/s10010-023-00627-0, 2023.

Miner, M. A.: Cumulative Damage in Fatigue, Journal of Applied Mechanics, 12, A159–A164, https://doi.org/10.1115/1.4009458, 1945.

Needelman, W. M. and Zaretsky, E. V.: Review of Rolling-Element Bearing Life Rating Methods, Tech. Rep. NASA/TM–2014-218141, National Aeronautics and Space Administration, Cleveland, OH, nASA Glenn Research Center; available from the NASA Technical Reports Server (NTRS), 2014.

O'Malley, T., Bursztein, E., Long, J., Chollet, F., Jin, H., Invernizzi, L., et al.: KerasTuner, https://github.com/keras-team/keras-tuner, 2019.

Pacheco, J., Pimenta, F., Guimarães, S., Castro, G., Álvaro Cunha, Matos, J. C., and Magalhães, F.: Experimental evaluation of fatigue in wind turbine blades with wake effects, Engineering Structures, 300, https://doi.org/https://doi.org/10.1016/j.engstruct.2023.117140, 2024.

Papadopoulos, K., Morfiadakis, E., Philippidis, T. P., and Lekou, D. J.: Assessment of the strain gauge technique for measurement of wind turbine blade loads, Wind Energy, 3, 35–65, https://doi.org/https://doi.org/10.1002/1099-1824(200001/03)3:1<35::AID-WE30>3.0.CO;2-D, 2000.

Pedregosa, F., Varoquaux, G., Gramfort, A., Michel, V., Thirion, B., Grisel, O., Blondel, M., Prettenhofer, P., Weiss, R., Dubourg, V., VanderPlas, J., Passos, A., Cournapeau, D., Brucher, M., Perrot, M., Duchesnay, E., et al.: scikit-learn: Machine Learning in Python, https://scikit-learn.org/, journal of Machine Learning Research, 12:2825–2830, 2011.

Pimenta, F., Ribeiro, D., Román, A., and Magalhães, F.: Predictive model for fatigue evaluation of floating wind turbines validated with experimental data, Renewable Energy, 223, 119 981, https://doi.org/https://doi.org/10.1016/j.renene.2024.119981, 2024.

Pulikollu, R., Haus, L., Mclaughlin, J., and Sheng, S.: Wind Turbine Main Bearing Reliability Analysis, Operations, and Maintenance Considerations: Electric Power Research Institute (EPRI), https://www.epri.com/research/products/000000003002029874, 2024.

Quick, J., Hart, E., Nilsen, M. B., Lund, R. S., Liew, J., Huang, P., Rethore, P.-E., Keller, J., Song, W., and Guo, Y.: Reductions in wind farm main bearing rating lives resulting from wake impingement, Wind Energy Science preprint, 2025, https://doi.org/10.5194/wes-2025-63.

Rinker, J. M., Hansen, M. H., and Larsen, T. J.: Calibrating a wind turbine model using diverse datasets, Journal of Physics: Conference Series, 1037, 062 026, https://doi.org/10.1088/1742-6596/1037/6/062026, 2018.

Rumelhart, D. E., Hinton, G. E., and Williams, R. J.: Learning representations by back-propagating errors, Nature, 323, 533–536, https://doi.org/10.1038/323533a0, 1986.

Sadeghi, N., Noppe, N., Morato, P. G., Weijtjens, W., and Devriendt, C.: Uncertainty quantification of wind turbine fatigue lifetime predictions through binning, Journal of Physics: Conference Series, 2767, 032 024, https://doi.org/10.1088/1742-6596/2767/3/032024, 2024.

Santos, F. D. N., Noppe, N., Weijtjens, W., and Devriendt, C.: Data-driven farm-wide fatigue estimation on jacket-foundation OWTs for multiple SHM setups, WIND ENERGY SCIENCE, 7, 299–321, https://doi.org/10.5194/wes-7-299-2022, 2022.

Schaeffler TPI-176: Lubrication of Rolling Bearings, Technical Product Information TPI 176, Schaeffler Technologies AG & Co. KG, Herzogenaurach, Germany, principles; Lubrication methods; Lubricant selection and testing; Storage and handling., 2014.

Schillaci, M. A.: Estimating the population variance, standard deviation and coefficient of variation: sample size and accuracy, Statistics & Probability Letters, 188, 110 420, https://doi.org/10.1016/j.spl.2022.110420, 2022.

Scribd: V52–850 kW Wind Turbine Technical Specification (Vestas Document), https://www.scribd.com/document/524089466/v52, accessed: 2025-10-29, 2021.

SKF Group: SKF Product Select – Single Bearing, https://productselect.skf.com/#/type-arrangement/single-bearing, accessed: 2025-10-27, 2025.

905 UNECE: Carbon Neutrality in the UNECE Region: Integrated Life-cycle Assessment of Electricity Sources, ECE Energy Series, United Nations, ISBN 978-92-1-001485-4, https://doi.org/10.18356/9789210014854, 2022.

Ziegler, L., Gonzalez, E., Rubert, T., Smolka, U., and Melero, J. J.: Lifetime extension of onshore wind turbines: A review covering Germany, Spain, Denmark, and the UK, Renewable and Sustainable Energy Reviews, 82, 1261–1271, https://doi.org/10.1016/j.rser.2017.09.100, 277 citations (Semantic Scholar/DOI) [2025-02-12], 2018.